Inorganic Chemistry

Article

pubs.acs.org/IC

What Controls the Sign and Magnitude of Magnetic Anisotropy in Tetrahedral Cobalt(II) Single-Ion Magnets?

Shefali Vaidya,[†] Subrata Tewary,[†] Saurabh Kumar Singh,[†] Stuart K. Langley,[‡] Keith S. Murray,[§] Yanhua Lan,[⊥] Wolfgang Wernsdorfer,[⊥] Gopalan Rajaraman,*[,†] and Maheswaran Shanmugam*[,†]

[†]Department of Chemistry, Indian Institute of Technology Bombay, Powai, Mumbai 400076, Maharashtra India

[‡]School of Science and the Environment, Chemistry Division, Manchester Metropolitan University, Manchester M15 6HB, U.K.

[§]School of Chemistry, Monash University, Clayton 3800, Victoria, Australia

[⊥]Institut Néel, CNRS and Université Grenoble Alpes, BP 166, 25 Avenue des Martyrs, 38042 Grenoble Cedex 9, France

Supporting Information

ABSTRACT: A family of mononuclear tetrahedral cobalt(II) thiourea complexes, $[Co(L_1)_4](NO_3)_2$ (**1**) and $[Co(L_x)_4](ClO_4)_2$ where x = 2 (**2**), 3 (**3**), 4 (**4**) (where L_1 = thiourea, L_2 = 1,3-dibutylthiourea, L_3 = 1,3-phenylethylthiourea, and L_4 = 1,1,3,3-tetramethylthiourea), has been synthesized using a rationally designed synthetic approach, with the aim of stabilizing an Ising-type magnetic anisotropy ($-D$). On the basis of direct-current, alternating-current, and hysteresis magnetic measurements and theoretical calculations, we have identified the factors that govern the sign and magnitude of D and ultimately the ability to design a single-ion magnet for a tetrahedral cobalt(II) ion. To better understand the magnetization relaxation dynamics, particularly for complexes **1** and **2**, dilution experiments were performed using their diamagnetic analogues, which are characterized by single-crystal X-ray diffraction with the general molecular formulas of $[Zn(L_1)_4](NO_3)_2$ (**5**) and $[Zn(L_2)_4](ClO_4)_2$ (**6**). Interestingly, intermolecular interactions are shown to play a role in quenching the quantum tunneling of magnetization in zero field, as evidenced in the hysteresis loop of **1**. Complex **2** exhibits the largest U_{eff} value of 62 cm^{-1} and reveals open hysteresis loops below 4 K. Furthermore, the influence of the hyperfine interaction on the magnetization relaxation dynamics is witnessed in the hysteresis loops, allowing us to determine the electron/nuclear spin $S(Co) = {}^3/_2/I(Co) = {}^7/_2$ hyperfine coupling constant of 550 MHz, a method ideally suited to determine the hyperfine coupling constant of highly anisotropic metal ions stabilized with large D value, which are otherwise hard to determine by conventional methods such as electron paramagnetic resonance.

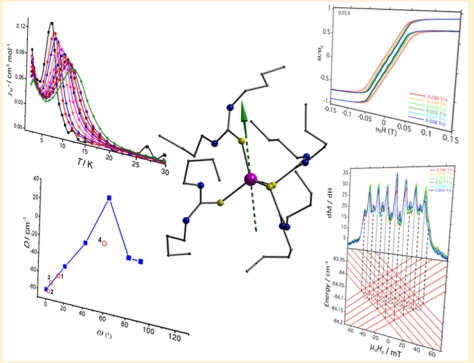

INTRODUCTION

Discrete molecular complexes with a magnetic ground state (S) coupled with Ising-type magnetic anisotropy ($-D$) present a barrier (U_{eff}) to reorient the magnetization vector. This situation leads to slow relaxation of the magnetization, and molecules that display this phenomenon have been termed single-molecule magnets (SMMs).[1] If slow relaxation of the magnetization originates from a mononuclear coordination complex, then it is often termed a single-ion magnet (SIM).[2] SMM/SIMs offer a potential application in high-density storage of digital data,[3] while the presence of quantum behavior such as quantum tunneling of magnetization (QTM),[1e] exchange bias,[4] and quantum coherence[5] makes these SMM/SIMs suitable candidates for realizing quantum computational and spintronics devices.[6] In order to realize molecular-based SIM/SMM devices, the parameters that dictate the behavior, S and D, need to be increased simultaneously and drastically in a controlled manner. Because $D \sim 1/S^2$, there is no easy way of manipulating simultaneously D and S.[7] In this article, we focus on the magnitude and sign of the D parameter in tetrahedral cobalt(II) complexes ($S = {}^3/_2$) by enhancing the orbital contributions to the spin. The majority of SMM or SIM compounds reported in the literature have been obtained serendipitously.[8] Although many research groups have proposed to have control over the spin-Hamiltonian (SH) parameters of complexes, particularly to modulate the D value,[9] still very little is known about the intricate factors that influence the magnitude and sign of the D value for any metal ion. This is particularly true for 3d transition-metal complexes because the orbital angular momentum is often quenched by the ligand field. Hence, a very limited number of SIMs have been reported based on 3d metal ions.[2a,10a−m] On the basis of a systematic investigation, we detailed not only how to control the sign of D but also the factors that significantly affect the magnitude of $-D$ in tetrahedral (T_d) cobalt(II) SIMs. We proposed recently that soft ligand donor atoms (such as sulfur), and metal−ligand covalency, hold the key to stabilizing a negative zero-field-

Received: May 3, 2016
Published: September 21, 2016

DOI: 10.1021/acs.inorgchem.6b01073
Inorg. Chem. 2016, 55, 9564−9578

splitting (zfs) parameter (D) in T_d cobalt(II) complexes.[11] To prove/confirm our proposed synthetic strategy to stabilize large negative D values, we have employed alternative sulfur-containing ligands, namely, thiourea and its derivatives L_1−L_4, where L_1 = thiourea, L_2 = 1,3-*n*-butylthiourea, L_3 = 1,3-phenylethylthiourea, and L_4 = 1,1,3,3-tetramethylthiourea (Scheme 1), to fine-tune the magnitude of the D value.

Scheme 1. Sulfur-Based Ligands (L_1−L_4) Employed To Isolate the T_d Cobalt(II) Complexes 1−4

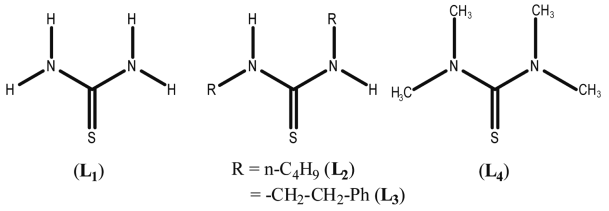

Using this controlled and rational synthetic approach, we report the isolation of several new cobalt(II)-based SIMs, with the largest anisotropy barrier for a T_d cobalt(II) complex.

EXPERIMENTAL AND COMPUTATIONAL METHODOLOGY

Unless otherwise stated, all of the reactions (both ligand and complex syntheses) were carried out under aerobic conditions, and all reagents were used as received without further purification. All of the ligands were purchased from a commercially available source (Alfa Aesar), except L_3, which was synthesized based on literature methods.[12] The formation and purity of the ligand was confirmed by electrospray ionization mass spectrometry and a Bruker 400 MHz NMR spectrophotometer. Magnetic susceptibility data (1.8−300 K) were collected on polycrystalline samples using a Quantum Design MPMS-XL SQUID magnetometer. Hysteresis loop measurements were performed on single crystals of **1**−**4** (both 100% and diluted samples in a diamagnetic matrix) with an array of micro-SQUIDs, in the temperature range of 0.04−5 K and in fields of up to 1.4 T, with sweep rates of up to 0.28 T s^{-1}. The external magnetic field is aligned parallel to the easy-axis of the complexes.[13] The time resolution is approximately 1 ms. The magnetic field can be applied in any direction of the micro-SQUID plane with a precision of much better than 0.1° by separately driving three orthogonal coils. In order to ensure good thermalization, each sample was fixed with apiezon grease.[13] The Zeeman diagram for complex **2** was generated by the *EasySpin* program adapted with the *Matlab R2014a* version. Ab initio calculations were performed using the *MOLCAS 7.8*[14] suite program and *ORCA*.[15] We have employed the [ANO-RCC···6s5p3d2f1g] basis set for cobalt, the [ANO-RCC···5s4p2d1f] basis set for sulfur, the [ANO-RCC···5s4p2d] basis set for nitrogen, the [ANO-RCC···4s3p2d] basis set for carbon, and the [ANO-RCC···2s1p] basis set for hydrogen. All complexes are four-coordinate with a distorted tetrahedral ($3d^7$) geometry around the metal center. Hence, the complexes possess an orbitally nondegenerate $^4A_2$ ground state. Mixing of the ground state with excited states via spin−orbit coupling leads to unquenched orbital momenta and Ising-type easy-axis anisotropy. Initially, we have performed CASSCF calculations on seven active electrons in five 3d orbitals (7,5) and further computed 10 quartets as well as 40 doublets states in the CI procedure. In the next step, we have mixed all 10 quartets and 40 doublets using the RASSI-SO module to compute the spin−orbit-coupled states. Further, these computed spin−orbit-coupled states were used to compute the **D** tensor and crystal-field parameters, as implemented in the *SINGLE_ANISO*[16] program. The Cholesky decomposition for two-electron integrals was employed throughout. State-average CASSCF calculations have been performed along with a second-order N-electron perturbation theory method, as implemented in the *ORCA 3.0.3* program package.[17] Scalar relativistic effects were included by the second-order Douglas−Kroll−Hess procedure.[18] An Ahlrichs all-electron relativistically polarized def2-TZVP basis set was used for calculation of the spin-free states.[19] The NEVPT2 calculations performed using *ORCA* were found to be in agreement with the *MOLCAS* procedures employed, and this offers confidence on the computed zfs values.

Caution! *Perchlorate salts are explosive in nature and should be handled in small amounts and carefully.*

Synthesis of $[Co(L_1)_4](NO_3)_2{\cdot}H_2O$ ***(1)***. $Co(NO_3)_2{\cdot}6H_2O$ (0.5 g, 1.7 mmol) was dissolved in a warm (T = 35−40 °C) solution of 1-butanol, followed by the addition of L_1 (0.522 g, 6.8 mmol), which was allowed to stir under reflux for 4 h. After that time, the reaction mixture was cooled to room temperature (RT), causing the crude product to precipitate. The crude was dissolved in ethyl acetate, and blue-green block-shaped crystals of **1** were grown from the filtrate after 3 days at 4 °C. Yield: 0.25 g (30%). Elem anal. Calcd (%): C, 9.51; H, 3.59; N, 27.71; S, 25.38. Found: C, 10.19; H, 3.42; N, 27.12; S, 25.63.

Synthesis of $[Co(L_2)_4](ClO_4)_2$ ***(2)***. $Co(ClO_4)_2{\cdot}6H_2O$ (0.5 g, 1.36 mmol) was dissolved in warm (T = 35−40 °C) ethyl acetate. To this was added L_2 (1.03 g, 5.4 mmol), and the reaction mixture was refluxed for 6 h. After that time, the reaction mixture was cooled to RT, and the solvent was removed under reduced pressure. The crude product was dissolved in 1-butanol, and blue-green block-shaped single crystals of **2** were grown from the filtrate after 3 days at −25 °C. Yield: 0.3 g (22%). Elem anal. Calcd (%): C, 42.76; H, 7.97; N, 11.08; S, 12.68. Found: C, 41.9; H, 7.42; N, 11.16; S, 12.16.

Synthesis of $[Co(L_3)_4](ClO_4)_2$ ***(3)***. The procedure for **2** was followed; however, L_3 (1.55 g, 5.4 mmol) was used in place of L_2. Yield: 0.2 g (10%). Elem anal. Calcd (%): C, 58.86; H, 5.58; N, 7.9; S, 9.04. Found: C, 57.94; H, 5.68; N, 8.13; S, 9.65.

Synthesis of $[Co(L_4)_4](ClO_4)_2$ ***(4)***. $Co(ClO_4)_2{\cdot}6H_2O$ (0.5 g, 1.36 mmol) was dissolved in a warm (T = 35−40 °C) solution of 2-propanol, followed by the addition of L_4 (0.725 g, 5.4 mmol), which was allowed to reflux for 6 h. The crude precipitate was collected by filtration upon cooling of the reaction mixture. This was redissolved in 2-propanol, and bluish-green single crystals of **4** began to grow from the filtrate after 24 h at 4 °C. Yield: 0.15 g (14%). Calcd: C, 42.76; H, 7.97; N, 11.08; S, 12.68. Found: C, 43.08; H, 7.52; N, 11.73; S, 13.16.

Synthesis of $[Zn(L_1)_4](NO_3)_2{\cdot}CH_3CN$ ***(5)***. $Zn(NO_3)_2{\cdot}6H_2O$ (0.978 g, 3.29 mmol) was dissolved in warm (T = 35−40 °C) solution of 1-butanol, followed by the addition of L_1 (1 g, 13.15 mmol), which was allowed to stir under reflux for 4 h. After that time, the reaction mixture was cooled to RT, and the solvent was removed under reduced pressure. Attempts to crystallize the complex of interest in ethyl acetate gave a single crystal, but it was not suitable for single-crystal X-ray diffraction. Hence, the polycrystalline sample was crystallized in acetonitrile, and blocked-shaped colorless crystals of **5** were grown at RT after 2 days. Yield: 3.2 g (42.6%). Elem anal. Calcd (%): C, 9.73; H, 3.27; N, 28.3; S, 25.97. Found: C, 9.73; H, 2.95; N, 28.48; S, 25.52.

Synthesis of $[Zn(L_2)_4](ClO_4)_2$ ***(6)***. $Zn(ClO_4)_2{\cdot}6H_2O$ (0.491 g, 1.33 mmol) was dissolved in warm (T = 35−40 °C) ethyl acetate, followed by the addition of L_2 (1 g, 5.31 mmol), which was allowed to stir under reflux for 6 h. After that time, the reaction mixture was cooled to RT, and the solvent was removed under reduced pressure. The crude was dissolved in 1-butanol, and white block-shaped crystals of **6** were grown from the filtrate after 3 days at −25 °C. Yield: 1.57 g (29%). Elem anal. Calcd (%): C, 42.49; H, 7.92; N, 11.01; S, 12.60. Found: C, 42.6; H, 7.56; N, 10.89; S, 12.42.

Preparation of a 10% Diluted Sample of ***1***. $CoNO_3{\cdot}6H_2O$ (0.096 g, 0.3289 mmol) and $ZnNO_3{\cdot}6H_2O$ (0.881g, 2.96 mmol) were dissolved in a warm (T = 35−40 °C) solution of 1-butanol, followed by the addition of L_1 (1 g, 13.2 mmol), which was allowed to stir under reflux for 4 h. After that time, the reaction mixture was cooled to RT, causing the crude product to precipitate (light blue in color). The crude was dissolved in ethyl acetate, and light-blue block-shaped crystals of a 10% diluted sample of **1** were grown from the filtrate after 5 days at 4 °C.

DOI: 10.1021/acs.inorgchem.6b01073
Inorg. Chem. 2016, 55, 9564−9578

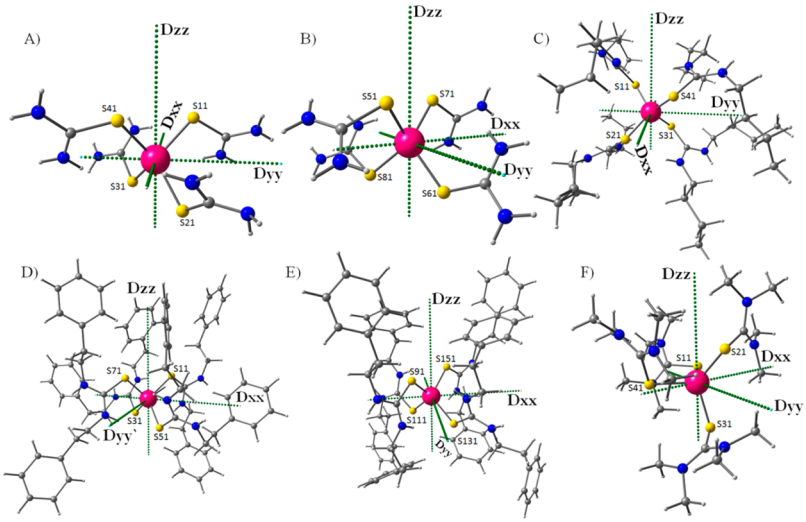

Figure 1. Ball-and-stick representations of the crystal structures along with *ab initio* computed orientation of *D*-tensor (A) **1a**, (B) **1b**, (C) **2**, (D) **3a**, (E) **3b**, and (F) **4**. Color code: magenta, Co; blue, N; gray, C.

Table 1. Crystallographic Data for Cmplexes 1−4

	1	2	3	4
formula	$Co_1C_4H_{18}N_{10}O_7S_4$	$Co_1C_{36}H_{80}N_8O_8S_4Cl_2$	$Co_1C_{69.5}H_{78.5}N_8S_4Cl_2O_{8.38}$	$Co_1C_{20}H_{48}N_8O_8S_4Cl_2$
size [mm]	0.23 × 0.2 × 0.15	0.25 × 0.23 × 0.20	0.31 × 0.29 × 0.16	0.23 × 0.21 × 0.06
system	monoclinic	triclinic	triclinic	monoclinic
space group	*Pc*	$P\bar{1}$	$P\bar{1}$	$P2_1/c$
a [Å]	17.380(4)	9.872(2)	12.680(3)	11.0016(17)
b [Å]	11.675(2)	12.827(3)	21.788(4)	11.0693(19)
c [Å]	9.717(19)	21.942(6)	26.086(4)	30.045(5)
α [deg]	90	89.409(1)	84.313(7)	90.0000
β [deg]	101.83(3)	79.215(7)	83.401(13)	99.965(4)
γ [deg]	90	70.307(6)	87.921(15)	90.0000
V [Å^3]	1929.8(7)	2565.6(11)	7122(2)	3603.7(10)
Z	4	2	2	4
ρ_{calcd}[g cm^{-3}]	1.740	1.309	1.322	1.450
$2\theta_{max}$	58.38	58.26	136.8	56.70
radiation	Mo K*α*	Mo K*α*	Cu K*α*	Mo K*α*
λ [Å]	0.71073	0.71073	1.54187	0.71073
T [K]	100	100	100	100
no. of reflns	27078	41311	79290	34082
no. of indep reflns	17172	13742	25231	8945
no. of reflns with $I > 2\sigma(I)$	8937	10736	21226	7767
R1	0.0383	0.0860	0.0730	0.0298
wR2	0.0752	0.1993	0.2112	0.0755

Preparation of a 15% Diluted Sample of **2**. $Co(ClO_4)_2·6H_2O$ (0.073 g, 0.2 mmol) and $Zn(ClO_4)_2·6H_2O$ (0.417 g, 1.13 mmol) were dissolved in warm (T = 35−40 °C) ethyl acetate, followed by the addition of L_2 (1 g, 5.31 mmol), which was allowed to stir under reflux for 6 h. After that time, the reaction mixture was cooled to RT, and the solvent was removed under reduced pressure. The crude was dissolved in 1-butanol, and light-blue block-shaped crystals of a 15% diluted sample of **2** were grown from the filtrate after 7 days at −25 °C.

Note: To confirm the dilution percentage, we performed UV−vis spectrometry of 100% samples of **1** (1×10^{-3} mol) and **2** (5×10^{-3} mol), and the corresponding diluted sample with the same concentration under similar experimental conditions in 1-butanol. The decreased intensity of spectral features for the diluted samples compared to the 100% sample of **1** and **2** is consistent with the dilution percentage (data not shown).

To check the phase purity of the bulk samples of **1**−**4**, powder X-ray diffraction (PXRD) was performed. The experimental PXRD pattern is in well agreement with that of the simulation data generated from its respective single-crystal X-ray diffraction (see Figure S1).

CCDC 1447664−1447667 for complexes **1**−**4**, respectively, and CCDC 1497492 and 1497493 for complexes **5** and **6**, respectively, are given in the Supporting Information. CIF files can be also downloaded free of charge at www.ccdc.cam.ac.uk/data_request/cif.

RESULTS AND DISCUSSION

The reaction of $Co(NO_3)_2·6H_2O$ or $Co(ClO_4)_2·6H_2O$ with ligands L_1−L_4 in alcoholic or ethyl acetate solutions yielded bluish-green block-shaped single crystals. Single-crystal X-ray diffraction experiments revealed the molecular formulas of these complexes to be $[Co(L_1)_4]NO_3·H_2O$ (**1**) and $[Co(L_x)_4](ClO_4)_2$, where x = 2 (**2**), 3 (**3**), 4 (**4**) (Figure 1). Complexes **1** and **4** crystallize in the monoclinic space groups *Pc* and $P2_1/c$, respectively, while complexes **2** and **3** both crystallize in the

DOI: 10.1021/acs.inorgchem.6b01073
Inorg. Chem. 2016, 55, 9564−9578

Table 2. Selected Bond Lengths (Å) and Bond Angles (deg) for 1−4

1a		1b		2	
Co1−S11	2.313(14)	Co2−S51	2.295(15)	Co1−S11	2.305(11)
Co1−S21	2.303(13)	Co2−S61	2.297(13)	Co1−S21	2.302(11)
Co1−S31	2.315(13)	Co2−S71	2.299(14)	Co1−S31	2.312(11)
Co1−S41	2.314(13)	Co2−S81	2.297(14)	Co1−S41	2.297(11)
S11−Co1−S21	125.08(5)	S51−Co2−S61	121.16(5)	S11−Co1−S21	115.88(4)
S11−Co1−S31	110.03(5)	S51−Co2−S71	112.87 (5)	S11−Co1−S31	95.99(4)
S11−Co1−S41	89.91(5)	S51−Co2−S81	92.11 (5)	S11−Co1−S41	116.55(4)
S21−Co1−S31	93.85(5)	S61−Co2−S71	89.97 (5)	S21−Co1−S31	114.75(4)
S21−Co1−S41	114.72(5)	S61−Co2−S81	118.24 (5)	S21−Co1−S41	95.34(4)
S31−Co1−S41	127.35(5)	S71−Co2−S81	125.4 (5)	S31−Co1−S41	119.89(4)
3a		**3b**		**4**	
Co1−S11	2.2919(12)	Co2−S91	2.2994(12)	Co1−S11	2.332(7)
Co1−S31	2.2828(12)	Co2−S111	2.3043(13)	Co1−S21	2.304(7)
Co1−S51	2.3064(12)	Co2−S131	2.3062(12)	Co1−S31	2.324(7)
Co1−S71	2.3070(12)	Co2−S151	2.3042(13)	Co1−S41	2.296(6)
S11−Co1−S31	115.23(5)	S91−Co2−S111	115.82(5)	S11−Co1−S21	104.51(16)
S11−Co1−S51	99.75(4)	S91−Co2−S131	97.87(4)	S11−Co1−S31	109.34(17)
S11−Co1−S71	115.97(5)	S91−Co2−S151	113.39(5)	S11−Co1−S41	104.94(17)
S31−Co1−S51	113.15(5)	S111−Co2−S131	113.26(5)	S21−Co1−S31	111.81(17)
S31−Co1−S71	99.12(4)	S111−Co2−S151	100.60(5)	S21−Co1−S41	120.72(18)
S51−Co1−S71	114.44(5)	S131−Co2−S151	116.80(5)	S31−Co1−S41	105.02(19)

triclinic space group $P\bar{1}$ (see Table 1). In all of the complexes, the cobalt ion is divalent with four sulfur-donor ligands directly coordinated to the metal ion, each exhibiting a distorted tetrahedral geometry (Figure 1), which is further reflected in their bond angles (see Table 2). The average Co−S bond lengths are 2.308(10), 2.304(11), 2.300(12), and 2.314(7) Å for **1**−**4**, respectively. Selected bond lengths and bond angles are listed in Table 2. The divalent cationic charge of the metal ion is neutralized by two nitrate anions for **1** and two perchlorate anions for **2**−**4**. The asymmetric unit of complex **1** consists of two crystallographically distinct molecules, which are labeled as **1a** and **1b** (Figure 1), whose structural parameters (Table 2) vary slightly.

The closest $Co^{II}\cdots Co^{II}$ distance in **1a**···**1a** is 7.215(5) Å, and that in **1b**···**1b** is 7.561(2) Å. In **1a**···**1b**, there are two distinct intermolecular distances, with these being 8.754(4) and 9.794(6) Å. When the distance is 8.754(4) Å, nitrate anions and water molecules reside between **1a** and **1b**. When the distance is 9.794(6) Å, only nitrate anions are found between two monomers. The nitrate anions and water molecules mediate several hydrogen-bonding interactions in multiple directions (Figure 2).

Similarly for complex **3**, the asymmetric unit consists of two crystallographically distinct molecules, which are labeled as **3a** and **3b** (Figure 1), and the structural parameters of **3a** and **3b** are very similar to each other (Table 2). The closest distance in **3a**···**3a** and **3b**···**3b** is found to be 12.680(2) Å. Again there are two different intermolecular distances observed in **3a**···**3b**, which are observed to be 14.659(4) and 12.855(2) Å.

Unlike in complex **1**, the perchlorate anions are located at the interface between the two **3a** molecules or two **3b** molecules. Because of the large size of the perchlorate anion compared to the nitrate anion in **1**, the distance in **3a**···**3a** [12.680(2) Å] or **3b**···**3b** [12.680(2) Å] is larger than those in **1a**···**1a** [7.215(5) Å] and **1b**···**1b** [7.561(2) Å] (see the packing diagram of **3** in Figure S3). The phenylethyl substituents on L_3 point toward

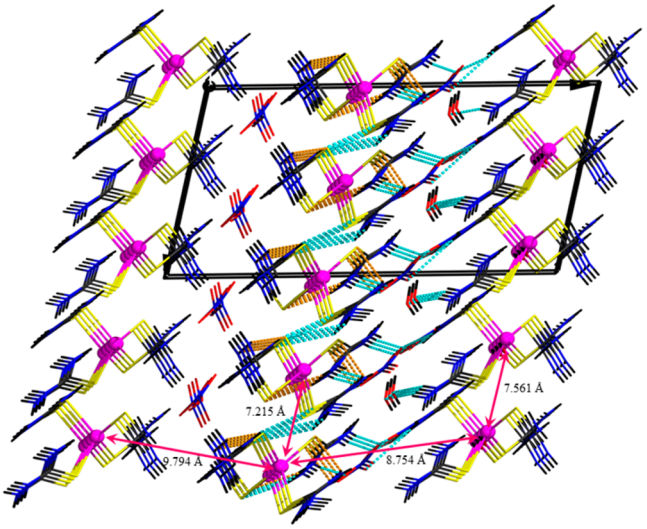

Figure 2. Packing diagram of complex **1**. Dotted sky-blue and orange-blue bonds represent the hydrogen-bonding network in complex **1**.

the interface of **3a**···**3b**, which leads to a drastic increase in the intermolecular distances [14.659(4) and 12.855(2) Å] in complex **3** compared to complex **1** (**1a**···**1b** distances in **1** were 8.754(4) and 9.794(6) Å; see Table 2). The intermolecular hydrogen bonding is mediated through the perchlorate anions; however, the strength of the hydrogen bonding in **3** is expected to be weaker than that in complex **1** because of the increased intermolecular distances.

In contrast to **1** and **3**, the asymmetric unit of complexes **2** and **4** consists of one distinct molecule, and the closest $Co^{II}\cdots Co^{II}$ distances were found to be 9.872(4) and 7.653(7) Å, respectively. In complexes **2** and **4**, both inter- and intramolecular hydrogen bonding is witnessed (see Figures S2 and S4), which are mediated through the perchlorate anions and ligated sulfur atom, respectively. The atoms involved in

DOI: 10.1021/acs.inorgchem.6b01073
Inorg. Chem. 2016, 55, 9564−9578

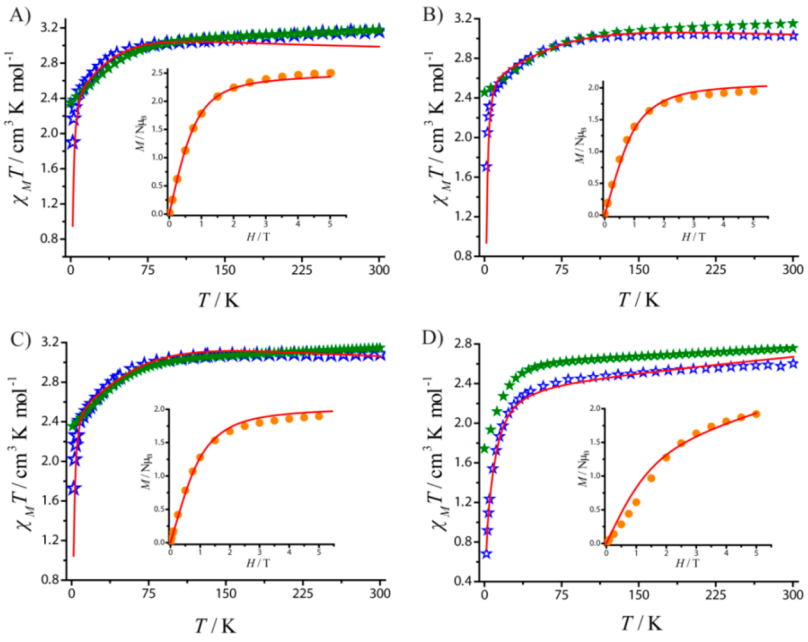

Figure 3. (A–D) Temperature-dependent magnetic susceptibility plots, with measurement performed on polycrystalline samples of **1–4**, respectively (H_{dc} = 1.0 T). Open star symbols (blue) represent the experimental magnetic data, and filled star symbols (green) represent $\chi_M T$ computed from CASSCF calculations. Insets: Field-dependent magnetization data collected on polycrystalline samples of complexes **1–4** at 2 K. The solid red lines represent the fits of the experimental magnetic data [$\chi_M T(T)$] and simulation of magnetization data using *PHI* sofware.[2b,11b,20]

Table 3. SH Parameters Extracted from the *PHI* Fitting[2b,11b,20,21] and Computed from the Ab Initio CASSCF+RASSI-SO Results from *MOLCAS*, Whereas the *ORCA* NEVPT2 Results Are in Parentheses, and the 2θ and ω Parameters Observed in Complexes 1–4[a]

complex	D_{fit}[b] (cm^{-1})	D_{cal}[c] (cm^{-1})	$\lvert E/D\rvert$[c] (cm^{-1})	g_{xx}, g_{yy}, g_{zz}[c]	torsion angle θ (deg)	2θ (deg)	dihedral angle ω (deg)
1a	−61.7	−62.8 (−55.5)	0.05 (0.04)	2.16, 2.26, 2.93 (2.10, 2.17, 2.78)	45.8	91.5	13.4
1b		−51.9 (−44.4)	0.05 (0.03)	2.18, 2.27, 2.84 (2.12, 2.15, 2.67)	45.5	91.0	18.1
2	−80.7	−84.0 (−69.7)	0.02 (0.01)	2.11, 2.16, 3.09 (2.08, 2.11, 2.90)	47.8	95.7	2.4
3a	−70.8	−63.8 (−48.2)	0.03 (0.02)	2.16, 2.23, 2.92 (2.12, 2.15, 2.71)	49.7	99.4	5.3
3b		−62.8 (−47.6)	0.03 (0.04)	2.17, 2.24, 2.92 (2.12, 2.17, 2.71)	49.6	99.2	2.7
4	−21.3	−21.5 (−15.2)	0.14 (0.12)	2.27, 2.35, 2.56 (2.19, 2.25, 2.38)	57.5	115.0	58

[a]The NEVPT2 computed zfs parameters for complex **3** are based on a model system (see the theoretical section for details). See the inset in Figure 12A for a description of θ and ω. [b]Extracted from the *PHI* fitting. [c]Computed from the ab initio CASSCF+RASSI-SO results from *MOLCAS*, whereas the *ORCA* NEVPT2 results are in parentheses.

mediating the inter- and intramolecular hydrogen bonding in all four complexes are listed in Tables S1–S4. Although complexes **2–4** show intermolecular hydrogen-bonding networks, the strength of the hydrogen bonding is expected to be stronger in **1** because of the short intermolecular $Co^{II}\cdots Co^{II}$ distances compared to those in the other complexes.

Direct-Current (dc) Magnetic Susceptibility Data of Complexes 1–4. Temperature-dependent dc magnetic susceptibility measurements were performed on polycrystalline samples for the four complexes between 2.0 and 300 K in the presence of an external magnetic field of 1.0 T (Figure 3). The RT $\chi_M T$ values of 3.10, 3.03, 3.08, and 2.60 cm^3 K mol^{-1} for complexes **1–4**, respectively, are significantly higher than the expected value for a mononuclear cobalt(II) ion with no first-order orbital angular momentum (1.875 cm^3 K mol^{-1}; g = 2).

As the temperature is reduced, the $\chi_M T$ value decreases gradually from RT to 50 K for **1**, **2**, and **4**, while the rate of decline is even greater for **3** in this temperature range. Below 50 K, the $\chi_M T$ value falls precipitously for all four complexes. These data unambiguously confirm that the magnetic anisotropy associated with these complexes is likely to be large and the temperature dependence from RT to 50 K is likely due to the depopulation of m_s levels. Field-dependent magnetization measurements were performed at 2, 4, and 8 K (for **1–4**), reaching values of 2.25, 1.99, 1.95, and 2.07 Nμ_B at 2.0 K and 5 T. In all cases, the magnetization was yet to saturate. The low moment values observed under low-temperature and high-field limits suggest that a significant anisotropy is found for each complex, which is backed up by the nonsuperimposable reduced magnetization curves (Figure S5).

For complexes **1–4**, the $\chi_M T(T)$ data were fitted using *PHI* software,[21] which resulted in reasonably good fits (Figure 3) and the extracted D values were used to simulate the $M(H)$ data of all of the complexes (Figure S6), which is in good agreement with the experimental data. The extracted D values are listed in Table 3. The extracted parameters are consistent with the literature reports.[2b,11b,20]

The results show that increasing the number of soft donor atoms around the tetrahedral cobalt(II) ion increases the magnitude of $-D$ (5-fold for **2**) compared to that of the monothione complex [$Co((Ph)_2N_4CS)Cl_2(MeCN)$] (**7**; D = −18 cm^{-1}), where the prediction was originally made.[11a] While

DOI: 10.1021/acs.inorgchem.6b01073
Inorg. Chem. 2016, 55, 9564–9578

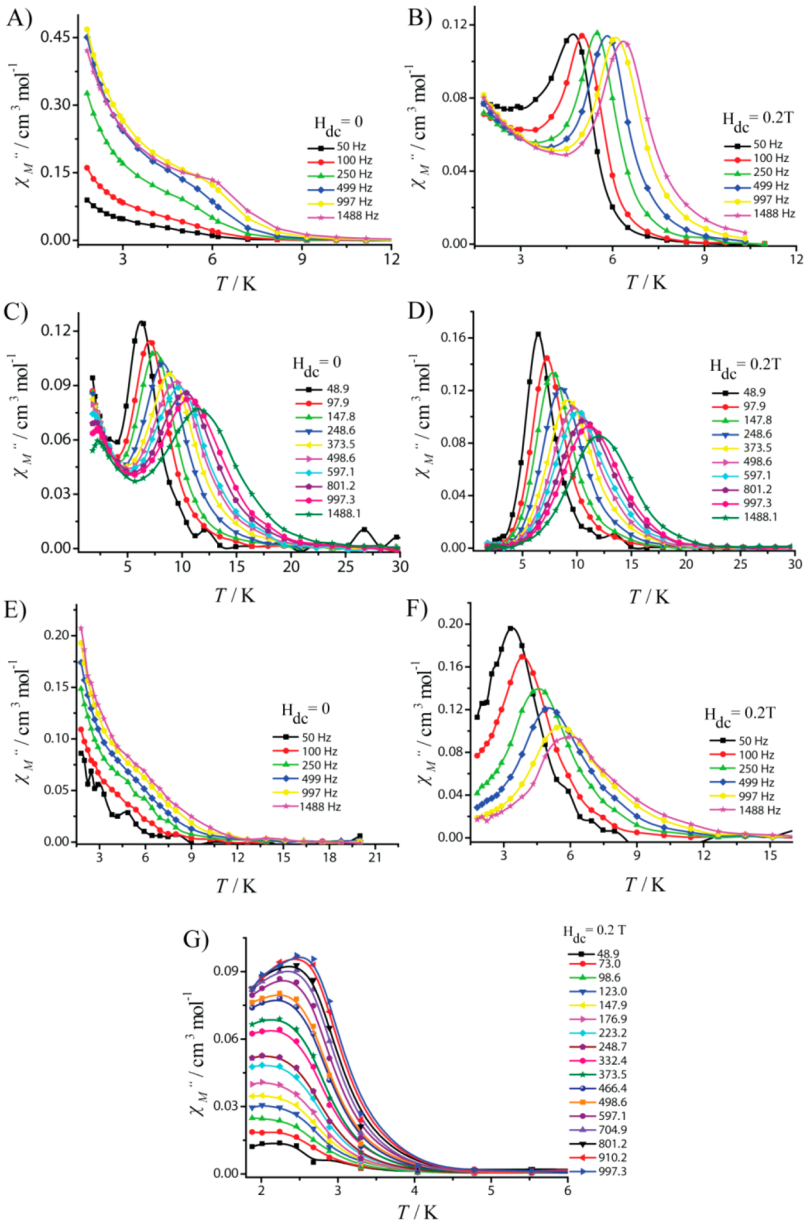

Figure 4. Frequency-dependent out-of-phase susceptibility signals for complexes **1**−**3** in zero dc field (panels A, C, and E, respectively) and in the presence of 0.2 T of a dc bias field for complexes **1**−**4** (panels B, D, F, and G, respectively).

each complex is structurally analogous, the SH parameters are significantly different, which was initially surprising to us. However, a detailed justification for this observation is described in the computational section (vide infra).

Alternating-Current (ac) Magnetic Susceptibility Data of Complexes 1−4. Because of the large anisotropy parameters, we tested each complex for SIM behavior via ac magnetic susceptibility measurements. These were performed on polycrystalline samples of **1**−**4** using a 3.5 Oe oscillating ac magnetic field, with and without an external magnetic field (Figures 4 and S7). Temperature- and frequency-dependent out-of-phase susceptibility signals (χ_M'') were observed for **1** in the absence of an external dc magnetic field (Figure 4A). This observation is in stark contrast with that for **7** (the monothione complex),[11a] where only field-induced SIM behavior was detected. The observation of zero-field SIM behavior in **1** provides further experimental evidence that increasing the number of soft donor ligands around the cobalt(II) ion (from one to four) increases the magnitude of $-D$ significantly.

Analysis of the ac data for **1** reveals that two relaxation processes are operative (Figures 4A and S7): a slow relaxation process between 3.5 and 10 K and a fast relaxation process below 3 K. The fast process at low temperatures is likely due to QTM, while the process at higher temperatures is a thermally activated process. The computed SH parameters (vide supra) evidently show that the $|E/D|$ ratio (0.05) is relatively low. In addition, complex **1** possesses a strong intermolecular interaction network. Non-negligible contributions are highly likely from both of these parameters (rhombicity and intermolecular interaction) for triggering the fast QTM behavior in **1**.

The existence of two different relaxations is consistent with the Cole−Cole plot constructed for complex **1** (Figure 5A), and the α values ranging from 0.11 to 0.01 (Table S5) indicate a narrow distribution of relaxation times. The Arrhenius plot

DOI: 10.1021/acs.inorgchem.6b01073
Inorg. Chem. 2016, 55, 9564−9578

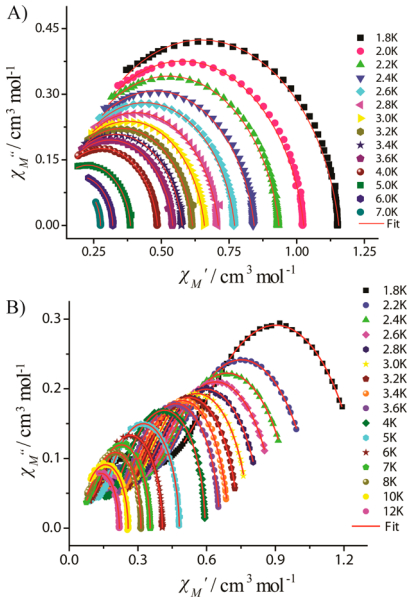

Figure 5. Cole−Cole plot of complexes (A) **1** and (B) **2** measured at the indicated temperature in a zero applied dc magnetic field. The red solid line is the best fit obtained using a generalized Debye model (see the text for details).

constructed from ac data of the thermally activated regime yielded a barrier to a magnetization reversal U_{eff} of 19.5 cm^{-1} ($\tau_0 = 7.59 \times 10^{-7}$s; Figure 6). The U_{eff} value observed for **1** is similar to those of the other tetrahedral cobalt(II) complexes reported in the literature.[2b,10g,11b]

In order to quench fast QTM[22] and to understand the influence of the supramolecular hydrogen-bonding interactions, ac measurements were performed in the presence of an external magnetic field of 0.2 T (100% sample; Figures 4B and S7) and

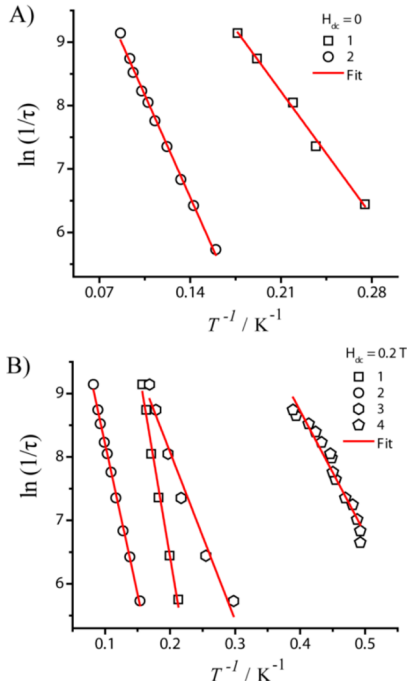

Figure 6. Arrhenius plot constructed from ac data for (A) complexes **1** and **2** in the absence of an external magnetic field and (B) complexes **1**−**4** in the presence of 0.2 T of an external magnetic field.

on a 10% sample of **1** diluted in a 90% (H_{dc} = 0) isostructural diamagnetic matrix (Figure 7A). Here we point out that,

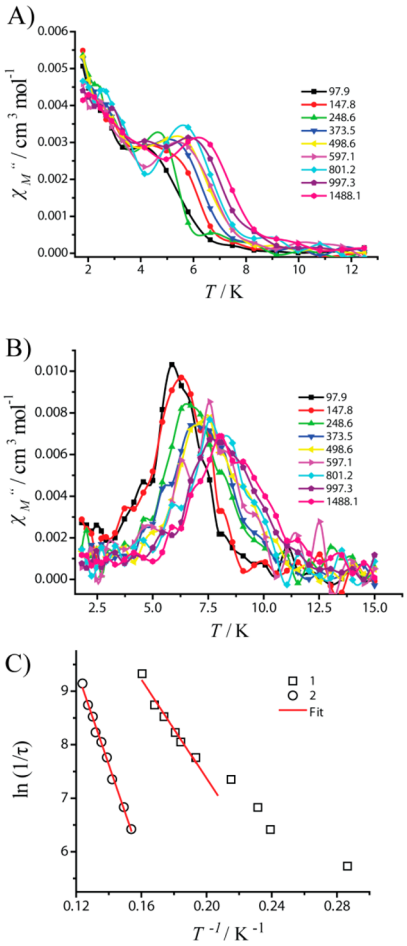

Figure 7. Frequency-dependent out-of-phase susceptibility signal of the 10% diluted samples of (A) **1** and (B) **2** in a zero external dc magnetic field at the indicated frequencies. (C) Arrhenius plot constructed from ac data for the 10% diluted samples of **1** and **2**.

although complex **5** (Figure S8 and Table S6) is structurally analogous to **1**, the crystals were grown in a different solvent (acetonitrile); therefore, the unit cell and packing diagram of **5** should be distinctly different from those of **1** (**1** crystallized from ethyl acetate). To prove that the unit cell and packing diagram of **5** are similar to those of **1**, PXRD was performed on the polycrystalline material obtained upon crystallization in ethyl acetate. Thus, the obtained PXRD pattern of **5** is in good agreement with the simulation (PXRD pattern generated from single-crystal data of **1**), emphasizing that complex **5** has structure and packing diagram similar to those of complex **1** (Figure S9). In both ac relaxation measurements, the peaks of the slow relaxation process observed at higher temperatures in the $\chi_M''(T)$ plot are now well resolved and the effective energy barrier increases to 42.4 cm^{-1} ($\tau_0 = 8.36 \times 10^{-9}$ s) and 32.3 cm^{-1} ($\tau_0 = 6.17 \times 10^{-8}$ s), respectively. There are multiple factors likely to be responsible for the increase of U_{eff}, such as the quenching of QTM to some extent and/or suppression of nuclear-spin-induced fast relaxation. A further dilution experiment confirms that the SIM behavior of **1** is of molecular origin rather than three-dimensional (3D) magnetic ordering.

DOI: 10.1021/acs.inorgchem.6b01073
Inorg. Chem. 2016, 55, 9564−9578

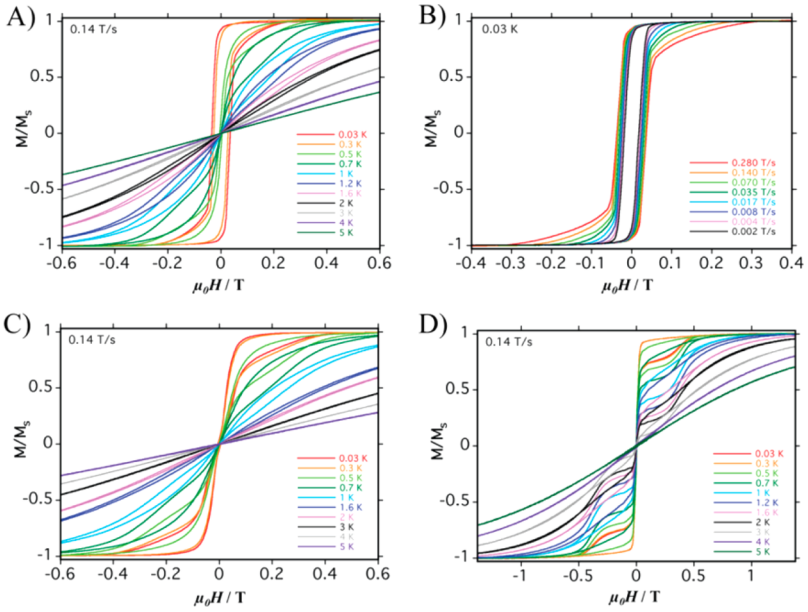

Figure 8. (A) Temperature- and (B) sweep-rate-dependent hysteresis loop measurements performed on a single crystal of **1** (100% sample), where a magnetic field applied in the average easy-axis directions of **1a** and **1b** molecules. (C) Field applied transverse to the average direction. (D) Measurements performed on a 10% diluted sample of **1**, where a magnetic field is applied parallel to the easy-axis of the molecule.

Alternatively, to reduce the intermolecular interactions in **1**, we decided to increase the interatomic distance and remove potential hydrogen-bonding donor sites from the L_1 ligand ($Co^{II}\cdots Co^{II}$ = 7.215 Å). Using this approach, we first isolated complex **4** [$Co^{II}\cdots Co^{II}$ = 7.653(7) Å] using a symmetrically substituted thiourea derivative [$(R_2N)_2CS$) (L_4), where R = methyl]. Interestingly, complex **4** does not display zero-field SIM behavior. The absence of a zero-field χ_M'' peak in **4** is likely due to the increased $|E/D|$ ratio (0.14) compared to that of **1** (see Table 3). The increased rhombicity could facilitate mixing of the ground state with the excited state and opens up underbarrier magnetization relaxation in full swing. However, ac measurements performed in the presence of a dc bias field (0.2 T) revealed χ_M'' signals with an effective energy barrier of 13.2 cm^{-1} (τ_0 = 3.21 × 10^{-8} s; Figures 4G and 6B). The significantly low $|E/D|$ ratio and strong supramolecular interaction in **1** compared to those in **4** plausibly play a significant role in quenching the QTM in zero magnetic field, if not completely, at least to a significant extent (vide infra).[4,23] Following this observation, we investigated the dynamic properties of **2** in which the cobalt(II) ion is coordinated by an unsymmetrically substituted thiourea ligand [$(HRN)_2CS$ (L_2), where R = *n*-butyl]. We found that the zero-field SIM behavior is reinstated (Figures 4C and S7), although the hydrogen-bonding strength is relatively weaker than that in **1** because of increased $Co^{II}\cdots Co^{II}$ separation (9.872 Å) compared to **1** (7.215 Å). Not only that, an effective energy barrier of 32.0 cm^{-1} (τ_0 = 2.24 × 10^{-6} s) was extracted from Arrhenius analysis of the ac data (Figure 6A).[8i]

Further, it is noticed that the U_{eff} parameter is significantly higher than that of complex **1** in a zero external magnetic field (100% sample), and this must be due to the significantly low $|E/D|$ ratio of **2** (0.02) compared to that of **1** (0.05) along with an increase in the $-D$ value, which is firmly supported by SH parameters extracted from magnetic data fitting (Table 3). Figure 4C illustrates again, however, that there is more than one relaxation process operational, as with **1** (Figure 5B and Table S7). Considering a significantly low $|E/D|$ ratio, the fast relaxation in **2** at lower temperature (Figure 4C and Figure S7) is presumably due to the intermolecular interactions and/or hyperfine interactions. In order to suppress/quench the fast relaxation process observed at low temperatures, ac data were collected for **2** in the presence of a 0.2 T dc magnetic field. In contrast to the scenario observed in **1**, the slow relaxation and frequency-dependent signals at higher temperatures (4.5−20 K) do not show any field dependence; i.e., there is no significant change in the extracted U_{eff} value, which was found to be 32.7 cm^{-1} with τ_0 = 2.49 × 10^{-6} s.

The fast relaxation observed at low temperature, however, is quenched completely (Figure 4D). To understand the nature of the dipolar interactions, ac susceptibility measurements (H_{dc} = 0) were performed on a 10% diluted sample [Figure 7B; 10% of **2** and 90% of the $[Zn(C_8H_{18}N_2H_2CS)_4]^{2+}$ diamagnetic analogue (Figure S8 and Table S6)]. The results clearly show frequency-dependent out-of-phase susceptibility signals. The anisotropic barrier extracted from an Arrhenius plot (Figure 7C) reveals a U_{eff} value of 62 cm^{-1} and τ_0 = 1.86 × 10^{-9} s, which is the largest value reported for any transition-metal-based SIM/SMMs with the exception of a two-coordinate iron(I) complex and a tetrahedral cobalt(II) complex.[20b,24]

Upon replacement of the *n*-butyl substituents in **2** by phenylethyl groups, it is found that the dynamic magnetic behavior of **3** is significantly different from that of **1**, **2**, and **4**. Out-of-phase susceptibility versus temperature plots reveal more than one relaxation process (one is below 3.5 K and the other at 3.5−9.0 K) in zero external magnetic field; however, none of the peaks are well-resolved, which hampers extraction of the energy barrier for magnetization reversal (Figure 4E). The significant change in the dynamic behavior of **3** compared to that of **2** is qualitatively ascertained by a reduced $-D$ value and increased $|E/D|$ value (Table 3). Ac data collected in the presence of a 0.2 T bias dc magnetic field (Figure 4F) lead to well-resolved χ_M'' peaks between 1.8 and 8.0 K. The effective energy barrier extracted was found to be 18.7 cm^{-1} with τ_0 = 1.55 × 10^{-6} s (Figure 6B). These observations clarify that not only the first coordination sphere but also the second

DOI: 10.1021/acs.inorgchem.6b01073
Inorg. Chem. 2016, 55, 9564−9578

coordination sphere has a significant influence in determining the magnitude of the D value (vide infra). Overall, in all of the complexes **1**−**4**, the experimentally extracted barrier from the Arrhenius plot is much lower than the theoretically expected energy barrier value. This is likely due to other competing relaxation mechanisms, such as QTM and two-phonon Raman processes.

Hysteresis Loop Measurements on Single Crystals of Complexes 1−4. In order to understand the influence of the 3D supramolecular interactions in **1** and to unequivocally confirm the SIM behavior, we performed hysteresis loop measurements on its single crystal using a μ-SQUID array. The easy axes of the two crystallographically distinct molecules **1a** and **1b** in the crystal lattice of **1** were found to orient in different directions (Figure 1). Complex **1** is crystallized in space group *Pc*. There are four molecules in an asymmetric unit, and a pair of crystallographically distinct molecules are generated by reflection. The two molecules are linked via hydrogen bonding, and the spins on these two molecules are canted at an angle of 25.6° and coupled by the presence of rather weak exchange interactions. Hence, the field is applied between these two distinct molecules rather than the pairs. Hysteresis loops open up at temperatures below 1.0 K when the external magnetic field is applied in the average projection of these two orientations, resulting in either antiferromagnetic or ferromagnetic interactions. The width of the hysteresis loops is strongly temperature- and sweep-rate-dependent (Figure 8A,B). In Figure 8A,B, the zero-field step increases very rapidly, indicative of ferromagnetic interactions. On the other hand, when the field is applied transverse to the average direction, the nature of interactions changes from ferromagnetic to antiferromagnetic because of the distinct orientations of magnetic anisotropy of these crystallographically distinct molecules.[25] This is unmistakably evidenced from the broadening zero-field step (Figure 8C).

Because of the resonance of the m_s levels and the occurrence of QTM, the first step in the hysteresis loop of an SMM/SIM is normally at zero field upon scanning from negative to positive fields. The presence of weak exchange-coupled neighboring antiferromagnetic interactions in complex **1** provides an exchange field that shifts the QTM step (resonance tunneling) to a new field position before zero. Indeed, the absence of a step at zero field (Figure 8C) with a shift to a field of H^* at −0.03 T in **1** confirms unambiguously the presence of antiferromagnetic interactions mediated by hydrogen bonding.[4,23] The strength of these intermolecular exchange interactions is estimated to be −0.014 cm^{-1} based on the equation $zJ' = g_z\mu_B H^* \cos(\Phi/2)/2S \cos \Phi$,[26] with Φ as an angle of easy axes between molecules **1a** and **1b** (25.6°) obtained from the theoretical calculation. Such a supramolecular interaction is too weak to transform the spin network into a classical magnet but allows for the quenching of QTM at zero field.

To further understand the role of hydrogen bonding in **1**, magnetic hysteresis measurements were performed on a single crystal of a 10% diluted sample of **1** (Figure 8D), where it is found that the magnetization relaxation becomes extremely fast at zero magnetic field suggesting that QTM is operating in full swing and no open loop is observed. This dilution experiment further confirms that the 3D ordering observed in **1** is mediated by the presence of supramolecular interactions via H-bonding and the SIM behavior is of molecular origin.

For complex **3**, the zero-field step in the hysteresis loop is very sharp, indicative of a fast tunneling rate. Indeed, because of the bulky phenylethyl groups on the ligand, the molecules are more isolated from each other, which reduces the intermolecular interactions. The zero-field step observed in the hysteresis loop of **3** upon scanning from a negative to a positive field is very similar to that found in a 10% diluted sample of **1**. Again, this measurement reiterates the point that intermolecular interaction is playing a crucial role in the quenching of QTM in **1** to some extent, while the weak nature of this interaction in **3** opens up the fast QTM. In complex **3**, a hysteresis loop opens below 3.0 K with strong temperature and sweep rate dependence, suggesting that this complex behaves as a SIM (Figures 9A and S10A).

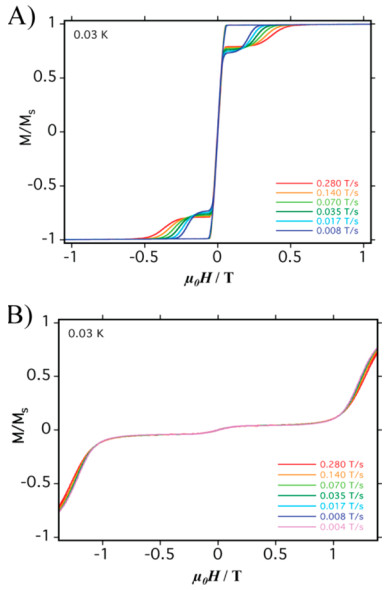

Figure 9. Sweep-rate-dependent hysteresis-loop measurements performed on single crystals of **3** (panel A) and **4** (panel B).

The increased blocking temperature in **3** compared to that in **1** is likely due to negligible deviation in the D_{zz} orientations between the crystallographically distinct molecules in **3** (3.3°, based on theoretical calculations) compared to that in **1** (25.6°; Figure S11). For complex **4**, there is no evidence for opening of the hysteresis loops (Figures 9B and S10B). The hysteresis loop is in a double S-shape, suggesting the presence of antiferromagnetic interactions between the molecules. The drastic change in the hysteresis behavior of **3** and **4** compared to that of **1** is likely due to the combined effects of supramolecular interactions and/or the reduced $-D$ value. In contrast to complexes **3** and **4**, the hysteresis loop of **2** begins to open below 4 K (Figure 10A,B) and the coercivity in this complex increases with decreasing temperature and increasing sweep rate. The coercivity of **2** increases further upon dilution with its diamagnetic analogue (Figure 10C,D). This suggests that dipolar interactions play a significant role in the relaxation dynamics in the 100% sample, which is also corroborated by the ac measurements.

There are several literature reports[8i,10e,27] claiming that the nuclear spin on the metal center can have a significant influence on the magnetization relaxation. However, experimentally this has not been seen in most cases because of smearing of the

DOI: 10.1021/acs.inorgchem.6b01073
Inorg. Chem. 2016, 55, 9564−9578

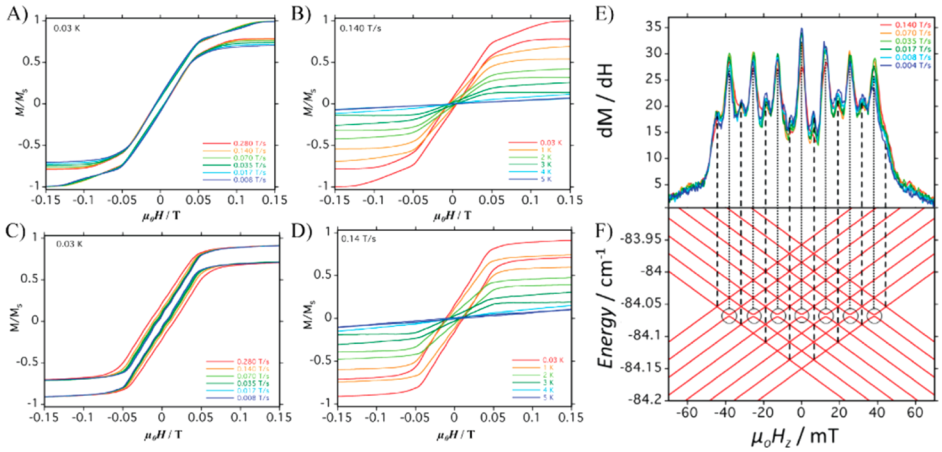

Figure 10. (A) Temperature- and (B) sweep-rate-dependent hysteresis loop measurement performed on a single crystal of complex **2** (100%). (C) Temperature- and (D) sweep-rate-dependent hysteresis loop measurement performed on a single crystal of a diluted sample of **2** (15%). (E) Field derivative of the hysteresis loops of a single crystal of a 15% diluted sample of **2** at 0.03 K, with sweep rates ranging from 0.140 to 0.004 T s^{-1}. (F) Zeeman diagram of the two times eight levels of the $I = {}^{7}/_{2}$ manifold of cobalt(II) in the field range of −70 to +70 mT as a function of the field H_z applied along the z axis. Resonant QTM occurs at the peaks of dM/dH. The corresponding level crossings are indicated as either dashed lines for a small tunneling splitting or dotted lines for a relatively large tunneling splitting. The crossing levels with larger tunneling splittings are highlighted by black circles, corresponding to the higher height of the dM/dH peaks.

quantum steps by dipolar interactions of the metal centers and/or inter- and intramolecular interactions.

Such a hyperfine interaction and its influence on magnetization relaxation dynamics has been witnessed in the 15% diluted sample of **2** (Figure 10C,D). As a result of the interactions between the electronic $S = {}^{3}/_{2}$ and nuclear $I = {}^{7}/_{2}$ spins of cobalt(II), 16 hyperfine levels, $2(2I + 1)$, should be observed with a constant spacing equal to the hyperfine coupling constant of A. Indeed, 15 steps are observed in the hysteresis loops at 0.03 K with different sweep rates at magnetic fields of 0, 0.006, 0.012, 0.019, 0.025, 0.032, 0.038, and 0.045 T and vice versa in the negative field range, as shown by the peaks of dM/dH versus μ_0H plots (Figure 10E).

The Zeeman diagram was generated by the *EasySpin* program based on the hyperfine Hamiltonian $AS{\cdot}I$ (Figure 10F). The 15 steps corresponding to the intersections between these levels are well reproduced with a hyperfine coupling constant A_{zz} of 550 MHz, using g_{zz} = 3.09 obtained from ab initio calculations (see Table 3). This value is comparable to, but a bit larger than, the one reported for a pseudotetrahedral cobalt(II) complex[28] having a similar CoS_4 metallic core. As shown in Figure 10E, the spacing between the hyperfine steps are almost equal but not for the height of the peaks. There are seven pronounced peaks with pairs of satellite peaks located on both sides. The pronounced hyperfine steps are evidenced by the crossing levels with a relatively large tunneling splitting (see the black circles in Figure 10F).

Computational Studies of Complexes 1−4. To rationalize the observed zfs parameters among the four structurally analogous complexes and to probe the origin of the differences observed, ab initio calculations (CASSCF+RASSI-SO) were performed on the X-ray structures of complexes **1**−**4**. The computed D_{zz} orientations for all of the complexes are shown in Figure 1 (see also Table S8). Except in complex **3**, in all other cases, the D_{zz} axis is found to bisect along the smaller ∠S−Co−S angle. Calculations predict the order **4** < **3** ∼ **1** < **2** for the magnitude of D (Table 3), and this trend is in agreement with the magnetic data simulation. The computed first spin-free excited states of all of the complexes reflect an order of **2** < **1** < **3** < **4**, and this is opposite to the trend observed for the magnitudes of the D values (see Table 4 for details). Among all four complexes, the first spin-free excited state is lowest in energy for complex **2**, and hence, a relatively large negative contribution to D value, leading to a giant zfs for this complex. To gain more insight into the origin of the zfs parameters and to understand the state-by-state contribution to the zfs parameters, additional calculations have been performed using the *ORCA* suite. Here, we have also incorporated the dynamic correlations by the means of NEVPT2 calculations. The computed SH parameters follow a trend similar to that of earlier theoretical observations and hence give confidence to the results. The additional SH parameters computed using *ORCA* code are provided in Table 3. We note here that, because of the large size of the molecule, the phenyl rings in complex **3** are modeled as hydrogen atoms to reduce the computational cost of performing NEVPT2 calculations.Therefore, the computed NEVPT2 results for this model system are smaller compared to the estimate obtained from CASSCF calculations when the full structure of complex **3** is used.

In tetrahedral (T_d) symmetry, the ^{4}F free-ion term of a cobalt(II) ion splits into the $^4A_2$ (ground state) and $^4T_2$ and $^4T_1$ terms (excited states). In T_d symmetry, the $^4T_2$(F) excited state is allowed to mix with the $^4A_2$ ground state, resulting in the existence of zfs in these complexes. However, any lowering from this symmetry leads to more rigorous mixing of the excited states and large D values. From Table 4, it is evident that for all of the complexes, the major contribution to the D value arises from the $^4T_2$(F) excited state. Because of lowering of the symmetry, these $^4T_2$(F) states further split and lead to different contributions from each excitation. Interestingly, the energy ordering of the first excited states in all four complexes follows the trend of the D value. Thus, the differences in the D value among all four complexes lie at the heart of the nature of structural distortion present in these complexes. Considering only the spin-conserved excitations, the negative D values arise from the transitions between the same $|m_l|$ levels that contribute to the axial anisotropy component $|D_{zz}|$. At the same time, transitions between different $|m_l|$ levels contribute to the

DOI: 10.1021/acs.inorgchem.6b01073
Inorg. Chem. 2016, 55, 9564−9578

Table 4. CASSCF-NEVPT2-Computed SH Parameters (g, D, and E) for 1−4 along with Statewise Contributions to the D Parameter Given in Parentheses[a]

	1a		1b		2		3a		3b		4	
	energy (cm^{-1})	contributions to the D value (cm^{-1})	energy (cm^{-1})	contributions to the D value (cm^{-1})	energy (cm^{-1})	contributions to the D value (cm^{-1})	energy (cm^{-1})	contributions to the D value (cm^{-1})	energy (cm^{-1})	contributions to the D value (cm^{-1})	energy (cm^{-1})	contributions to the D value (cm^{-1})
$^4T_2(F)$	1319.5 (902.3),	−75.7	1639.2 (1062.3),	−63.680	1031.6 (715.6),	−90.207	1542.1 (995.4),	−68.6	1481.8 (989.5),	−68.6	3537.7 (2311.1),	−35.1
	5576.3	(−98.7),	6127.2	(−88.7),	6219.9	(−112.3),	5385.4	(−92.0),	5543.7	(−92.4),	4118.0	(−52.2),
	(3750.1),	9.6 (14.1),	(4110.5),	8.108 (12.0),	(4173.3),	8.272 (12.2),	(3987.3),	8.74 (12.8),	(3746.0),	9.39 (13.7),	(2706.9),	10.8 (16.2),
	7205.6 (4743.6)	1.4 (2.1)	7133.4 (4749.6)	4.603 (6.8)	7141.0 (4765.5)	4.370 (6.5)	7213.8 (4658.0)	5.61 (8.4)	7002.1 (4642.9)	4.5 (6.7)	5909.2 (3948.9)	9.02 (13.4)
D_{tot}		−55.4		−44.4 (−60.5)		−69.73 (−83.2)		−48.2		−47.6		−15.2
		(−69.43)						(−62.4)		(−61.8)		(−21.3)
$\lvert E/D \rvert$		0.04 (0.04)		0.03 (0.03)		0.01 (0.01)		0.02 (0.02)		0.03 (0.03)		0.11 (0.13)

[a]The values given parentheses are for CASSCF calculations performed using the *ORCA* suite.

positive D values.[29] The cobalt(II) ion has an $e^4t_2^3$ configuration, and mixing of the $^4T_2(F)$ excited state occurs through excitation of a single electron from the e subshell to the t_2 subshell ($e^3t_2^4$). Thus, the largest negative D contribution to the D value is essentially due to the transition between the $d_{x^2-y^2}$ (e subshell) and d_{xy} (t_2 subshell) levels. Neese and co-workers[30] have recently proposed that the sign of the D parameter also depends on the energies of d_{z^2} and $d_{x^2-y^2}$ orbitals. Their work detailed that the larger the energy differences between these orbitals, the greater the contribution toward a negative D parameter.

The presence of the largest negative D value observed in **2** is essentially due to the certain specific structural distortion present in this complex. A closer look into the structural description suggests that a D_{2d} point group is a more realistic group theoretical notation for **2** than the T_d notation. Thus, the presence of D_{2d} symmetry in **2** leads to splitting of $^4T_2(F)$ into $^4B_2$ and ^4E, with a significant lowering of the $^4B_2$ level to very close to the $^4B_1$ level (Figure 11). This is accordance with the energy trend observed for complex **2**, with the first excited state being very close to the ground state (1031.6 cm^{-1}), followed by two other excited states at ∼7000 cm^{-1}. Because of a very low-lying first excited state ($^4B_2$), the contribution from this excited state is significantly large (∼−90 cm^{-1}), leading to an overall giant magnetic anisotropy for this complex. Moreover, the computed orbital ordering also follows the same trend and explains that such a large negative contribution arising from $^4B_1 \rightarrow {}^4B_2$ is essentially due to the transition from $d_{x^2-y^2}$ to d_{xy}. The deviation from ideal D_{2d} symmetry can be roughly correlated to a difference in the magnitude of the D values for all complexes (vide infra). On the other hand, complex **4** possesses a 4-fold smaller D value compared to the largest D value reported for **2**. A key difference has been noticed between the splitting patterns of the $^4T_2(F)$ level of **2** and **4**. In stark contrast to the splitting pattern of **2**, the $^4T_2(F)$ level of **4** splits in a near-symmetrical fashion with a first excited state (∼5000 cm^{-1}) 5 times higher in energy than that of complex **2** (Figure S12). Thus, one may expect a smaller D value for **4**. This difference is attributed to distortion in the geometry because complex **4** is strongly distorted from D_{2d} symmetry (closer to T_d symmetry).

On the basis of structural data, two key parameters are found to be responsible for altering the orbital energies: one is the torsion angle (2θ) and the other is the dihedral angle (ω), as defined in the inset of Figure 12A. The 2θ and ω values for complexes **1**−**4** are listed in Table 3. To further understand the role of these parameters in estimating the zfs, we have developed a correlation by varying the 2θ parameter (Figure 12A), where a large negative D value is observed for a smaller 2θ parameter. Although the experimental data points are in agreement with the correlation developed (Figure 12A), it is very clear that this parameter alone cannot explain the trend in the magnitude of the D value observed because of the slight variation in 2θ among all of the complexes.

To understand the role of the second coordination sphere on D, another correlation is developed by varying the ω parameter (Figure 12B). A larger deviation in ω tends to decrease the negative D value. At 60°, the sign of D switches from negative to positive in nature, while a distortion beyond this value (>60°) again results in a negative D parameter. The experimentally extracted D values fit well within the correlation developed (Figure 12B). This scenario unequivocally establishes that the second coordination sphere also possesses an equally important contribution to control not only the sign but

DOI: 10.1021/acs.inorgchem.6b01073
Inorg. Chem. 2016, 55, 9564−9578

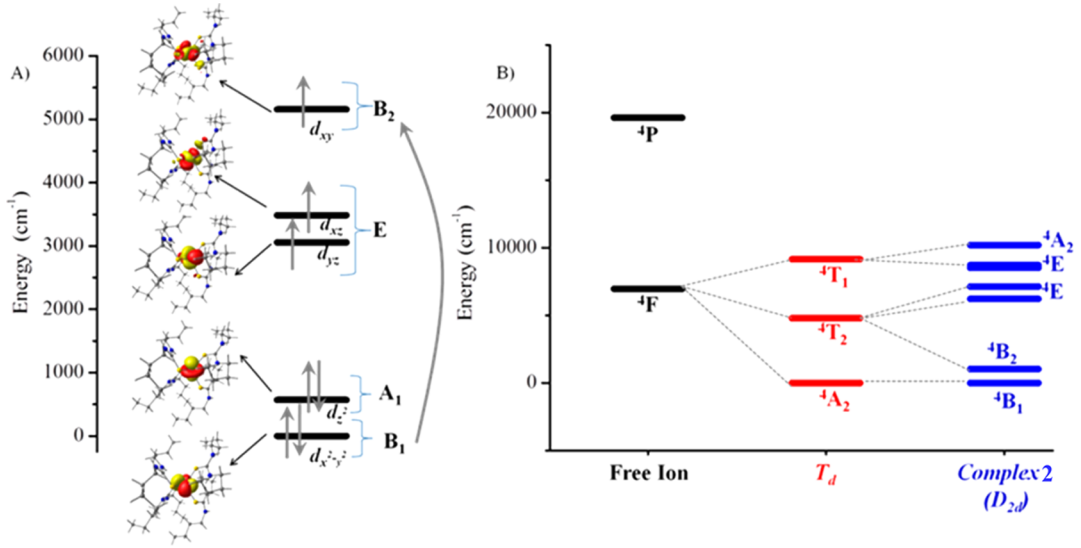

Figure 11. (A) CASSCF-computed d-orbital ordering for complex **2**. The main anisotropic axes have been chosen as a reference frame. The isodensity surface represented here corresponds to a cutoff value of 0.023 e bohr^{-3} (left). (B) NEVPT2-computed energies of a low-lying quartet state for complex **2** along with the ideal T_d complex.

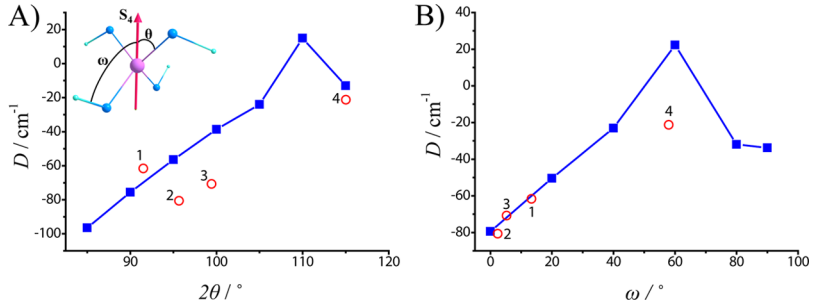

Figure 12. Magnetostructural correlation developed based on the torsion angle (2θ) and dihedral angle (ω) for complex **1** (inset of panel A) by varying (A) the 2θ parameter and (B) the ω parameter (blue lines). The inset in part A describes the two parameters defined for complexes **1**–**4**. The red open circles represent the experimental D values extracted for complexes **1**–**4** from magnetic data fitting.

also the magnitude of the D value. We note here that in the developed correlation average values for the θ and ω parameters (Table 3) are given. However, as noted (Tables 3 and S9), the individual values vary significantly in some cases, and one has to take this into consideration for future predictions on the sign and magnitude of D values.[30a]

We accentuate that the theoretical prediction on the influence of the secondary coordination sphere[30a] on the D value has been verified experimentally for the first time. We found that the interaction between the π orbital of the coordinated sulfur and the π^* antibonding orbital of cobalt(II) is responsible for orbital ordering. This interaction is totally governed by the 2θ and ω parameters. A larger deviation in 2θ/ω leads to an unfavorable overlap between the π orbitals of sulfur and the cobalt(II) $d_{x^2-y^2}$ orbital, leading to stabilization of the π^* orbital of cobalt(II). This results in small $E(d_{z^2}) - E(d_{x^2-y^2})$ and large $E(d_{x^2-y^2}) - E(d_{xy})$ energy gaps and a small negative D value.[30a] A small deviation has the opposite effect, with a large negative D value expected. Among the four complexes, **2** shows the smallest 2θ and ω deviations, while **4** shows the largest deviations (Table 3). The total deviations for complexes **1** and **3** are as expected from the experiment found between that of **2** and **4**. The experimentally observed trend in the D value is therefore in accordance with the theoretical calculations.

CONCLUSION

In conclusion, we have synthesized four new cobalt(II) SIMs, with distorted tetrahedral geometries using a rationally designed approach, using soft donor ligands. Despite the fact that all four complexes possess the $[CoS_4]$ core, the D value was found to vary from −21 to −84 cm^{-1}. Ab initio calculations performed validate the sign and magnitude of D and suggest that the variation in D originates from the first and second coordination sphere interactions. Interestingly, the influence of the second coordination sphere on the magnitude of D is found to be very significant, leading to the observation of zero-field SMM behavior with the largest U_{eff} observed for any transition-metal complex, in **2**, while in the case of **4**, only field-induced SMM behavior is observed. The presence of supramolecular interactions, via hydrogen bonding, is found to quench the QTM effects to some extent, resulting in open hysteresis loops for **1**. Complex **2** displays open hysteresis loops below 4 K, where, evidently, the rare influence of the cobalt nuclear spin on the magnetization relaxation is witnessed. This allowed us to extract the hyperfine coupling constant directly from a hysteresis loop measurement, which is a very unique observation in SMM/SIM chemistry. Overall, the proposed rational synthetic approach leads to improved magnetic behavior and offers a way to enhance the D value (thus

DOI: 10.1021/acs.inorgchem.6b01073
Inorg. Chem. 2016, 55, 9564−9578

increased U_{eff}) and to achieve a new generation of tetrahedral cobalt(II) SIMs.

■ ASSOCIATED CONTENT

Supporting Information

The Supporting Information is available free of charge on the ACS Publications website at DOI: 10.1021/acs.inorgchem.6b01073.

Structural parameters, supporting magnetic data (both bulk and single crystal), and computational details (PDF)
CCDC 1447664 for **1** (CIF)
CCDC 1447665 for **2** (CIF)
CCDC 1447666 for **3** (CIF)
CCDC 1447667 for **4** (CIF)
CCDC 1497492 for **5** (CIF)
CCDC 1497493 for **6** (CIF)

■ AUTHOR INFORMATION

Corresponding Authors

*E-mail: rajaraman@chem.iitb.ac.in (G.R.).
*E-mail: eswar@chem.iitb.ac.in (M.S.).

Notes

The authors declare no competing financial interest.

■ ACKNOWLEDGMENTS

M.S. thanks the funding agencies DST, DST Nanomission, INSA, and IIT Bombay for financial support. Y.L. and W.W. acknowledge the EU for financial support within the FP7 FET-Proactive Project MoQuaS No. 610449 and for the Agence Nationale de la Recherche for Project MolQuSpin No. ANR-13-BS10. S.V. and S.K.S. thank the CSIR for fellowships, and S.T. thanks the UGC for a fellowships. Y.L. thanks Dr. Eufemio Pineda for helpful assistance in using the *EasySpin* program. G.R. and K.S.M. thank the Australia−India AISRF program for support.

■ REFERENCES

(1) (a) Sessoli, R.; Gatteschi, D.; Caneschi, A.; Novak, M. A. Magnetic bistability in a metal-ion cluster. *Nature* **1993**, *365*, 141−3. (b) Sessoli, R.; Tsai, H. L.; Schake, A. R.; Wang, S.; Vincent, J. B.; Folting, K.; Gatteschi, D.; Christou, G.; Hendrickson, D. N. High-spin molecules: [Mn12O12(O2CR)16(H2O)4]. *J. Am. Chem. Soc.* **1993**, *115*, 1804−16. (c) Gatteschi, D.; Caneschi, A.; Pardi, L.; Sessoli, R. Large clusters of metal ions: the transition from molecular to bulk magnets. *Science* **1994**, *265*, 1054−1058. (d) Winpenny, R., Ed. *Single-Molecule Magnets and Related Phenomena*; Springer: New York, 2006; p 262 pp. (e) Gatteschi, D.; Sessoli, R.; Villain, J. *Molecular Nanomagnets*; Oxford University Press: Oxford, U.K., 2006.

(2) (a) Harman, W. H.; Harris, T. D.; Freedman, D. E.; Fong, H.; Chang, A.; Rinehart, J. D.; Ozarowski, A.; Sougrati, M. T.; Grandjean, F.; Long, G. J.; Long, J. R.; Chang, C. J. Slow Magnetic Relaxation in a Family of Trigonal Pyramidal Iron(II) Pyrrolide Complexes. *J. Am. Chem. Soc.* **2010**, *132*, 18115−18126. (b) Zadrozny, J. M.; Long, J. R. Slow Magnetic Relaxation at Zero Field in the Tetrahedral Complex [Co(SPh)4]2. *J. Am. Chem. Soc.* **2011**, *133*, 20732−20734. (c) Freedman, D. E.; Harman, W. H.; Harris, T. D.; Long, G. J.; Chang, C. J.; Long, J. R. Slow Magnetic Relaxation in a High-Spin Iron(II) Complex. *J. Am. Chem. Soc.* **2010**, *132* (4), 1224−1225.

(3) Christou, G.; Gatteschi, D.; Hendrickson, D. N.; Sessoli, R. Single-molecule magnets. *MRS Bull.* **2000**, *25*, 66−71.

(4) (a) Wernsdorfer, W.; Aliaga-Alcalde, N.; Hendrickson, D. N.; Christou, G. Exchange-biased quantum tunnelling in a supramolecular dimer of single-molecule magnets. *Nature* **2002**, *416*, 406−409. (b) Wernsdorfer, W.; Aliaga-Alcalde, N.; Tiron, R.; Hendrickson, D. N.; Christou, G. Quantum dynamics of exchange biased single-molecule magnets. *J. Magn. Magn. Mater.* **2004**, *272*−*276*, 1037−1041. (c) Nguyen, T. N.; Wernsdorfer, W.; Shiddiq, M.; Abboud, K. A.; Hill, S.; Christou, G. Supramolecular aggregates of single-molecule magnets: exchange-biased quantum tunneling of magnetization in a rectangular [Mn3]4 tetramer. *Chem. Sci.* **2016**, *7*, 1156−1173. (d) Nguyen, T. N.; Wernsdorfer, W.; Abboud, K. A.; Christou, G. A Supramolecular Aggregate of Four Exchange-Biased Single-Molecule Magnets. *J. Am. Chem. Soc.* **2011**, *133*, 20688−20691. (e) Nava, A.; Rigamonti, L.; Zangrando, E.; Sessoli, R.; Wernsdorfer, W.; Cornia, A. Redox-Controlled Exchange Bias in a Supramolecular Chain of Fe4 Single-Molecule Magnets. *Angew. Chem., Int. Ed.* **2015**, *54*, 8777−8782.

(5) (a) Yang, J.; Wang, Y.; Wang, Z.; Rong, X.; Duan, C.-K.; Su, J.-H.; Du, J. Observing quantum oscillation of ground states in single molecular magnet. *Phys. Rev. Lett.* **2012**, *108*, 230501−230505. (b) Chang, B.; Wang, Q.; Xie, H.; Liang, J. Q. Macroscopic quantum coherence in a single molecular magnet and Kondo effect of electron transport. *Phys. Lett. A* **2011**, *375*, 2932−2938. (c) Schlegel, C.; van Slageren, J.; Manoli, M.; Brechin, E. K.; Dressel, M. Direct Observation of Quantum Coherence in Single-Molecule Magnets. *Phys. Rev. Lett.* **2008**, *101* (14), 147201−147204. (d) Abeywardana, C.; Mowson, A. M.; Christou, G.; Takahashi, S. Spin coherence in a Mn3 single-molecule magnet. *Appl. Phys. Lett.* **2016**, *108*, 042401−042404.

(6) (a) Westerstroem, R.; Dreiser, J.; Piamonteze, C.; Muntwiler, M.; Weyeneth, S.; Kraemer, K.; Liu, S. X.; Decurtins, S.; Popov, A.; Yang, S.; Dunsch, L.; Greber, T. Tunneling, remanence, and frustration in dysprosium based endohedral single molecule magnets. *Phys. Rev. B: Condens. Matter Mater. Phys.* **2014**, *89*, 060406−060409. (b) Jenkins, M.; Hummer, T.; Martinez-Perez, M. J.; Garcia-Ripoll, J.; Zueco, D.; Luis, F. Coupling single molecule magnets to quantum circuits. *New J. Phys.* **2013**, *15*, 095007−095028. (c) Leuenberger, M. N.; Loss, D. Quantum computing in molecular magnets. *Nature* **2001**, *410*, 789−793. (d) Lehmann, J.; Gaita-Arino, A.; Coronado, E.; Loss, D. Spin qubits with electrically gated polyoxometalate molecules. *Nat. Nanotechnol.* **2007**, *2*, 312−317. (e) Bogani, L.; Wernsdorfer, W. Molecular spintronics using single-molecule magnets. *Nat. Mater.* **2008**, *7*, 179−186. (f) Sessoli, R.; Boulon, M.-E.; Caneschi, A.; Mannini, M.; Poggini, L.; Wilhelm, F.; Rogalev, A. Strong magneto-chiral dichroism in a paramagnetic molecular helix observed by hard X-rays. *Nat. Phys.* **2014**, *11*, 69−74.

(7) Neese, F.; Pantazis, D. A. What is not required to make a single molecule magnet. *Faraday Discuss.* **2011**, *148*, 229−238.

(8) (a) Murrie, M. Cobalt(ii) single-molecule magnets. *Chem. Soc. Rev.* **2010**, *39*, 1986−1995. (b) Rosado Piquer, L.; Sanudo, E. C. Heterometallic 3d-4f single-molecule magnets. *Dalton Trans.* **2015**, *44*, 8771−8780. (c) Sessoli, R.; Powell, A. K. Strategies towards single molecule magnets based on lanthanide ions. *Coord. Chem. Rev.* **2009**, *253*, 2328−2341. (d) Ishikawa, N.; Sugita, M.; Ishikawa, T.; Koshihara, S.-Y.; Kaizu, Y. Lanthanide Double-Decker Complexes Functioning as Magnets at the Single-Molecular Level. *J. Am. Chem. Soc.* **2003**, *125*, 8694−8695. (e) Langley, S. J.; Helliwell, M.; Sessoli, R.; Rosa, P.; Wernsdorfer, W.; Winpenny, R. E. P. Slow relaxation of magnetisation in an octanuclear cobalt(II) phosphonate cage complex. *Chem. Commun.* **2005**, 5029−5031. (f) Langley, S.; Helliwell, M.; Sessoli, R.; Teat, S. J.; Winpenny, R. E. P. Synthesis and structural and magnetic characterization of cobalt(II)-sodium phosphonate cage compounds. *Dalton Trans.* **2009**, 3102−3110. (g) Novikov, V. V.; Pavlov, A. A.; Nelyubina, Y. V.; Boulon, M.-E.; Varzatskii, O. A.; Voloshin, Y. Z.; Winpenny, R. E. P. A Trigonal Prismatic Mononuclear Cobalt(II) Complex Showing Single-Molecule Magnet Behavior. *J. Am. Chem. Soc.* **2015**, *137*, 9792−9795. (h) Milios, C. J.; Vinslava, A.; Wernsdorfer, W.; Moggach, S.; Parsons, S.; Perlepes, S. P.; Christou, G.; Brechin, E. K. A Record Anisotropy Barrier for a Single-Molecule Magnet. *J. Am. Chem. Soc.* **2007**, *129*, 2754−2755. (i) Fataftah, M. S.; Zadrozny, J. M.; Rogers, D. M.; Freedman, D. E. A Mononuclear Transition Metal Single-Molecule Magnet in a Nuclear Spin-Free Ligand Environment. *Inorg. Chem.* **2014**, *53*, 10716−10721. (j) Woods, T. J.; Ballesteros-Rivas, M. F.; Ostrovsky, S. M.; Palii, A.

DOI: 10.1021/acs.inorgchem.6b01073
Inorg. Chem. 2016, 55, 9564−9578

V.; Reu, O. S.; Klokishner, S. I.; Dunbar, K. R. Strong Direct Magnetic Coupling in a Dinuclear CoII Tetrazine Radical Single-Molecule Magnet. *Chem. - Eur. J.* **2015**, *21*, 10302−10305. (k) Palii, A. V.; Reu, O. S.; Ostrovsky, S. M.; Klokishner, S. I.; Tsukerblat, B. S.; Sun, Z.-M.; Mao, J.-G.; Prosvirin, A. V.; Zhao, H.-H.; Dunbar, K. R. A Highly Anisotropic Cobalt(II)-Based Single-Chain Magnet: Exploration of Spin Canting in an Antiferromagnetic Array. *J. Am. Chem. Soc.* **2008**, *130*, 14729−14738. (l) Palii, A. V.; Ostrovsky, S. M.; Klokishner, S. I.; Reu, O. S.; Sun, Z.-M.; Prosvirin, A. V.; Zhao, H.-H.; Mao, J.-G.; Dunbar, K. R. Origin of the Single Chain Magnet Behavior of the Co(H2L)(H2O) Compound with a 1D Structure. *J. Phys. Chem. A* **2006**, *110* (51), 14003−14012. (m) Brown, A. J.; Pinkowicz, D.; Saber, M. R.; Dunbar, K. R. A Trigonal-Pyramidal Erbium(III) Single-Molecule Magnet. *Angew. Chem., Int. Ed.* **2015**, *54*, 5864−5868.

(9) (a) Idesicova, M.; Titis, J.; Krzystek, J.; Boca, R. Zero-Field Splitting in Pseudotetrahedral Co(II) Complexes: a Magnetic, High-Frequency and -Field EPR, and Computational Study. *Inorg. Chem.* **2013**, *52*, 9409−9417. (b) Papankova, B.; Boca, R.; Dlhan, L.; Nemec, I.; Titis, J.; Svoboda, I.; Fuess, H. Magneto-structural relationships for a mononuclear Co(II) complex with large zero-field splitting. *Inorg. Chim. Acta* **2010**, *363*, 147−156.

(10) (a) Gomez-Coca, S.; Aravena, D.; Morales, R.; Ruiz, E. Large magnetic anisotropy in mononuclear metal complexes. *Coord. Chem. Rev.* **2015**, *289*−*290*, 379−392. (b) Shao, F.; Cahier, B.; Guihery, N.; Riviere, E.; Guillot, R.; Barra, A.-L.; Lan, Y.; Wernsdorfer, W.; Campbell, V. E.; Mallah, T. Tuning the Ising-type anisotropy in trigonal bipyramidal Co(II) complexes. *Chem. Commun.* **2015**, *51*, 16475−16478. (c) Bar, A. K.; Pichon, C.; Sutter, J.-P. Magnetic anisotropy in two- to eight-coordinated transition-metal complexes: Recent developments in molecular magnetism. *Coord. Chem. Rev.* **2016**, *308*, 346−380. (d) Craig, G. A.; Murrie, M. 3d single-ion magnets. *Chem. Soc. Rev.* **2015**, *44*, 2135−2147. (e) Ruamps, R.; Batchelor, L. J.; Guillot, R.; Zakhia, G.; Barra, A.-L.; Wernsdorfer, W.; Guihery, N.; Mallah, T. Ising-type magnetic anisotropy and single molecule magnet behaviour in mononuclear trigonal bipyramidal Co(II) complexes. *Chem. Sci.* **2014**, *5*, 3418−3424. (f) Zadrozny, J. M.; Liu, J.; Piro, N. A.; Chang, C. J.; Hill, S.; Long, J. R. Slow magnetic relaxation in a pseudotetrahedral cobalt(II) complex with easy-plane anisotropy. *Chem. Commun.* **2012**, *48*, 3927−3929. (g) Saber, M. R.; Dunbar, K. R. Ligands effects on the magnetic anisotropy of tetrahedral cobalt complexes. *Chem. Commun.* **2014**, *50*, 12266−12269. (h) Cornia, A.; Rigamonti, L.; Boccedi, S.; Clerac, R.; Rouzieres, M.; Sorace, L. Magnetic blocking in extended metal atom chains: a pentachromium(II) complex behaving as a single-molecule magnet. *Chem. Commun.* **2014**, *50*, 15191−15194. (i) Deng, Y.-F.; Han, T.; Wang, Z.; Ouyang, Z.; Yin, B.; Zheng, Z.; Krzystek, J.; Zheng, Y.-Z. Uniaxial magnetic anisotropy of square-planar chromium(II) complexes revealed by magnetic and HF-EPR studies. *Chem. Commun.* **2015**, *51*, 17688−17691. (j) Sato, R.; Suzuki, K.; Minato, T.; Shinoe, M.; Yamaguchi, K.; Mizuno, N. Field-induced slow magnetic relaxation of octahedrally coordinated mononuclear Fe(III)-, Co(II)-, and Mn(III)-containing polyoxometalates. *Chem. Commun.* **2015**, *51*, 4081−4084. (k) Craig, G. A.; Marbey, J. J.; Hill, S.; Roubeau, O.; Parsons, S.; Murrie, M. Field-Induced Slow Relaxation in a Monometallic Manganese(III) Single-Molecule Magnet. *Inorg. Chem.* **2015**, *54*, 13−15. (l) Grigoropoulos, A.; Pissas, M.; Papatolis, P.; Psycharis, V.; Kyritsis, P.; Sanakis, Y. Spin-Relaxation Properties of a High-Spin Mononuclear MnIIIO6-Containing Complex. *Inorg. Chem.* **2013**, *52*, 12869−12871. (m) Marriott, K. E. R.; Bhaskaran, L.; Wilson, C.; Medarde, M.; Ochsenbein, S. T.; Hill, S.; Murrie, M. Pushing the limits of magnetic anisotropy in trigonal bipyramidal Ni(II). *Chem. Sci.* **2015**, *6*, 6823−6828.

(11) (a) Vaidya, S.; Upadhyay, A.; Singh, S. K.; Gupta, T.; Tewary, S.; Langley, S. K.; Walsh, J. P. S.; Murray, K. S.; Rajaraman, G.; Shanmugam, M. A synthetic strategy for switching the single ion anisotropy in tetrahedral Co(II) complexes. *Chem. Commun.* **2015**, *51*, 3739−3742. (b) Zadrozny, J. M.; Telser, J.; Long, J. R. Slow magnetic relaxation in the tetrahedral cobalt(II) complexes [Co(EPh)4]2- (EO, S, Se). *Polyhedron* **2013**, *64*, 209−217.

(12) Maddani, M. R.; Prabhu, K. R. A concise synthesis of substituted thiourea derivatives in aqueous medium. *J. Org. Chem.* **2010**, *75*, 2327−2332.

(13) (a) Wernsdorfer, W.; Chakov, N. E.; Christou, G. Determination of the magnetic anisotropy axes of single-molecule magnets. *Phys. Rev. B: Condens. Matter Mater. Phys.* **2004**, *70*, 132411−132414. (b) Wernsdorfer, W. From micro- to nano-SQUIDs: applications to nanomagnetism. *Supercond. Sci. Technol.* **2009**, *22* (6), 064013.

(14) (a) Karlstroem, G.; Lindh, R.; Malmqvist, P.-A.; Roos, B. O.; Ryde, U.; Veryazov, V.; Widmark, P.-O.; Cossi, M.; Schimmelpfennig, B.; Neogrady, P.; Seijo, L. MOLCAS: a program package for computational chemistry. *Comput. Mater. Sci.* **2003**, *28*, 222−239. (b) Veryazov, V.; Widmark, P.-O.; Serrano-Andres, L.; Lindh, R.; Roos, B. O. 2MOLCAS as a development platform for quantum chemistry software. *Int. J. Quantum Chem.* **2004**, *100*, 626−635. (c) Aquilante, F.; De Vico, L.; Ferre, N.; Ghigo, G.; Malmqvist, P.-a.; Neogrady, P.; Pedersen, T. B.; Pitonak, M.; Reiher, M.; Roos, B. O.; Serrano-Andres, L.; Urban, M.; Veryazov, V.; Lindh, R. MOLCAS 7: The Next Generation. *J. Comput. Chem.* **2010**, *31*, 224−247. (d) Duncan, J. A. Molcas 7.2. *J. Am. Chem. Soc.* **2009**, *131* (6), 2416.

(15) (a) Neese, F.; Petrenko, T.; Ganyushin, D.; Olbrich, G. Advanced aspects of ab initio theoretical optical spectroscopy of transition metal complexes: Multiplets, spin-orbit coupling and resonance Raman intensities. *Coord. Chem. Rev.* **2007**, *251*, 288−327. (b) Neese, F. The ORCA program system. *Wiley Interdisciplinary Reviews-Computational Molecular Science* **2012**, *2*, 73−78. (c) Neese, F. *ORCA*; University of Bonn: Bonn, Germany, 2010.

(16) Chibotaru, L. F.; Ungur, L. Ab initio calculation of anisotropic magnetic properties of complexes. I. Unique definition of pseudo spin Hamiltonians and their derivation. *J. Chem. Phys.* **2012**, *137*, 064112.

(17) (a) Angeli, C.; Cimiraglia, R.; Evangelisti, S.; Leininger, T.; Malrieu, J. P. Introduction of n-electron valence states for multireference perturbation theory. *J. Chem. Phys.* **2001**, *114*, 10252−10264. (b) Angeli, C.; Cimiraglia, R.; Malrieu, J.-P. N-electron valence state perturbation theory: a fast implementation of the strongly contracted variant. *Chem. Phys. Lett.* **2001**, *350*, 297−305. (c) Angeli, C.; Cimiraglia, R. Multireference perturbation configuration interaction V. Third-order energy contributions in the M?ller-Plesset and Epstein-Nesbet partitions. *Theor. Chem. Acc.* **2002**, *107*, 313−317. (d) Angeli, C.; Cimiraglia, R.; Malrieu, J.-P. n-electron valence state perturbation theory: a spinless formulation and an efficient implementation of the strongly contracted and of the partially contracted variants. *J. Chem. Phys.* **2002**, *117*, 9138−9153.

(18) Hess, B. A. Relativistic electronic-structure calculations employing a two-component no-pair formalism with external-field projection operators. *Phys. Rev. A: At., Mol., Opt. Phys.* **1986**, *33*, 3742−8.

(19) (a) Schaefer, A.; Huber, C.; Ahlrichs, R. Fully optimized contracted Gaussian basis sets of triple zeta valence quality for atoms Li to Kr. *J. Chem. Phys.* **1994**, *100*, 5829−35. (b) Weigend, F.; Ahlrichs, R. Balanced basis sets of split valence, triple zeta valence and quadruple zeta valence quality for H to Rn: Design and assessment of accuracy. *Phys. Chem. Chem. Phys.* **2005**, *7*, 3297−3305. (c) Schaefer, A.; Horn, H.; Ahlrichs, R. Fully optimized contracted Gaussian basis sets for atoms lithium to krypton. *J. Chem. Phys.* **1992**, *97*, 2571−7.

(20) (a) Eichhoefer, A.; Lan, Y.; Mereacre, V.; Bodenstein, T.; Weigend, F. Slow Magnetic Relaxation in Trigonal-Planar Mononuclear Fe(II) and Co(II) Bis(trimethylsilyl)amido Complexes-A Comparative Study. *Inorg. Chem.* **2014**, *53*, 1962−1974. (b) Rechkemmer, Y.; Breitgoff, F. D.; Neugebauer, P.; van Slageren, J.; van der Meer, M.; Sarkar, B.; Atanasov, M.; Neese, F.; Hakl, M.; Orlita, M. A four-coordinate cobalt(II) single-ion magnet with coercivity and a very high energy barrier. *Nat. Commun.* **2016**, *7*, 10467−10474.

(21) Chilton, N. F.; Anderson, R. P.; Turner, L. D.; Soncini, A.; Murray, K. S. PHI: A powerful new program for the analysis of anisotropic monomeric and exchange-coupled polynuclear d- and f-block complexes. *J. Comput. Chem.* **2013**, *34*, 1164−1175.

(22) Sessoli, R.; Gatteschi, D.; Wernsdorfer, W. Quantum Tunneling of the Magnetization in Molecular Nanoclusters. In *Quantum*

DOI: 10.1021/acs.inorgchem.6b01073
Inorg. Chem. 2016, 55, 9564−9578

Phenomena in Clusters and Nanostructures; Khanna, S. N., Castleman, A. W., Eds.; Springer: Berlin, 2003; pp 55−82.
(23) (a) Yang, E.-C.; Wernsdorfer, W.; Hill, S.; Edwards, R. S.; Nakano, M.; Maccagnano, S.; Zakharov, L. N.; Rheingold, A. L.; Christou, G.; Hendrickson, D. N. Exchange bias in Ni4 single-molecule magnets. *Polyhedron* **2003**, *22*, 1727−1733. (b) Pinkowicz, D.; Southerland, H. I.; Avendano, C.; Prosvirin, A.; Sanders, C.; Wernsdorfer, W.; Pedersen, K. S.; Dreiser, J.; Clerac, R.; Nehrkorn, J.; Simeoni, G. G.; Schnegg, A.; Holldack, K.; Dunbar, K. R. Cyanide Single-Molecule Magnets Exhibiting Solvent Dependent Reversible ″On″ and ″Off″ Exchange Bias Behavior. *J. Am. Chem. Soc.* **2015**, *137*, 14406−14422. (c) Inglis, R.; Jones, L. F.; Mason, K.; Collins, A.; Moggach, S. A.; Parsons, S.; Perlepes, S. P.; Wernsdorfer, W.; Brechin, E. K. Ground spin state changes and 3D networks of exchange coupled [MnIII3] single-molecule magnets. *Chem. - Eur. J.* **2008**, *14*, 9117−9121. (d) Das, A.; Gieb, K.; Krupskaya, Y.; Demeshko, S.; Dechert, S.; Klingeler, R.; Kataev, V.; Buchner, B.; Muller, P.; Meyer, F. A New Family of 1D Exchange Biased Heterometal Single-Molecule Magnets: Observation of Pronounced Quantum Tunneling Steps in the Hysteresis Loops of Quasi-Linear {Mn2Ni3} Clusters. *J. Am. Chem. Soc.* **2011**, *133*, 3433−3443. (e) Bagai, R.; Wernsdorfer, W.; Abboud, K. A.; Christou, G. Exchange-Biased Dimers of Single-Molecule Magnets in OFF and ON States. *J. Am. Chem. Soc.* **2007**, *129*, 12918−12919.
(24) Zadrozny, J. M.; Xiao, D. J.; Atanasov, M.; Long, G. J.; Grandjean, F.; Neese, F.; Long, J. R. Magnetic blocking in a linear iron(I) complex. *Nat. Chem.* **2013**, *5*, 577−581.
(25) Liu, J.; Chen, Y.-C.; Liu, J.-L.; Vieru, V.; Ungur, L.; Jia, J.-H.; Chibotaru, L. F.; Lan, Y.; Wernsdorfer, W.; Gao, S.; Chen, X.-M.; Tong, M.-L. A Stable Pentagonal Bipyramidal Dy(III) Single-Ion Magnet with a Record Magnetization Reversal Barrier over 1000 K. *J. Am. Chem. Soc.* **2016**, *138*, 5441−5450.
(26) Lecren, L.; Wernsdorfer, W.; Li, Y.-G.; Roubeau, O.; Miyasaka, H.; Clerac, R. Quantum Tunneling and Quantum Phase Interference in a [MnII2MnIII2] Single-Molecule Magnet. *J. Am. Chem. Soc.* **2005**, *127*, 11311−11317.
(27) (a) Gomez-Coca, S.; Urtizberea, A.; Cremades, E.; Alonso, P. J.; Camon, A.; Ruiz, E.; Luis, F. Origin of slow magnetic relaxation in Kramers ions with non-uniaxial anisotropy. *Nat. Commun.* **2014**, *5*, 4300−4307. (b) Ishikawa, N.; Sugita, M.; Wernsdorfer, W. Nuclear Spin Driven Quantum Tunneling of Magnetization in a New Lanthanide Single-Molecule Magnet: Bis(Phthalocyaninato)holmium Anion. *J. Am. Chem. Soc.* **2005**, *127*, 3650−3651.
(28) Maganas, D.; Milikisyants, S.; Rijnbeek, J. M. A.; Sottini, S.; Levesanos, N.; Kyritsis, P.; Groenen, E. J. J. A Multifrequency High-Field Electron Paramagnetic Resonance Study of CoIIS4 Coordination. *Inorg. Chem.* **2010**, *49*, 595−605.
(29) Gomez-Coca, S.; Cremades, E.; Aliaga-Alcalde, N.; Ruiz, E. Mononuclear Single-Molecule Magnets: Tailoring the Magnetic Anisotropy of First-Row Transition-Metal Complexes. *J. Am. Chem. Soc.* **2013**, *135*, 7010−7018.
(30) (a) Suturina, E. A.; Maganas, D.; Bill, E.; Atanasov, M.; Neese, F. Magneto-Structural Correlations in a Series of Pseudotetrahedral [CoII(XR)4]2- Single Molecule Magnets: An ab Initio Ligand Field Study. *Inorg. Chem.* **2015**, *54*, 9948−9961. (b) Maganas, D.; Sottini, S.; Kyritsis, P.; Groenen, E. J. J.; Neese, F. Theoretical Analysis of the Spin Hamiltonian Parameters in Co(II)S4 Complexes, Using Density Functional Theory and Correlated ab initio Methods. *Inorg. Chem.* **2011**, *50*, 8741−8754.

DOI: 10.1021/acs.inorgchem.6b01073
Inorg. Chem. 2016, 55, 9564−9578